Circuits and Systems
Mekelweg 4,
2628 CD Delft
The Netherlands
http://ens.ewi.tudelft.nl/

CAS-2014-4257715

M.Sc. Thesis

Indoor Granular Presence Sensing and Control Messaging with an Ultrasonic Circular Array Sensor

Shahrzad Naghibzadeh

Abstract

Providing automated granular control of lighting, along with user-driven control, results in an energy-efficient smart lighting system design while catering to personal occupant preferences. Two functional ingredients in such a system are: (i) sensing that provides granular information on occupant location, and (ii) a communication system to transmit control messages from a user. We consider an ultrasonic circular array sensor that provides the dual functionality of granular occupant sensing and a communication receiver for user control transmissions. A ceiling-mounted sensor configuration with a co-located ultrasonic transmitter and array receiver is considered. Algorithms for localization and tracking of an occupant in an indoor environment is presented.The resulting occupant location and tracks may be used for energy-efficient lighting. In addition, a user may control lighting by sending messages at a near-ultrasonic frequency through a mobile device, which are processed by the receiver array, and used to adapt a requested parameter of the lighting system. The proposed sensing and messaging solution is tested in an indoor office space with an 8-element receiver array sensor prototype. The efficacy of both systems is evaluated empirically and through simulations.

Indoor Granular Presence Sensing and Control Messaging with an Ultrasonic Circular Array Sensor

Thesis

submitted in partial fulfillment of the
requirements for the degree of

Master of Science

in

Electrical Engineering

by

Shahrzad Naghibzadeh
born in Mashhad, Iran

This work was performed in:

Philips Research, Nat.Lab. Group
Philips Research Europe
High Tech Campus 34
5656 AE Eindhoven, The Netherlands

Delft University of Technology

Delft University of Technology
Department of
Telecommunications

The undersigned hereby certify that they have read and recommend to the Faculty of Electrical Engineering, Mathematics and Computer Science for acceptance a thesis entitled **"Indoor Granular Presence Sensing and Control Messaging with an Ultrasonic Circular Array Sensor"** by **Shahrzad Naghibzadeh** in partial fulfillment of the requirements for the degree of **Master of Science**.

Dated: July 16, 2014

Advisors:

Dr.ir. Ashish Pandharipande

Prof.dr.ir. Geert Leus

Committee Member:

Dr.ir.Marco Zuniga

Abstract

Providing automated granular control of lighting, along with user-driven control, results in an energy-efficient smart lighting system design while catering to personal occupant preferences. Two functional ingredients in such a system are: (i) sensing that provides granular information on occupant location, and (ii) a communication system to transmit control messages from a user. We consider an ultrasonic circular array sensor that provides the dual functionality of granular occupant sensing and a communication receiver for user control transmissions. A ceiling-mounted sensor configuration with a co-located ultrasonic transmitter and array receiver is considered. Algorithms for localization and tracking of an occupant in an indoor environment is presented.The resulting occupant location and tracks may be used for energy-efficient lighting. In addition, a user may control lighting by sending messages at a near-ultrasonic frequency through a mobile device, which are processed by the receiver array, and used to adapt a requested parameter of the lighting system. The proposed sensing and messaging solution is tested in an indoor office space with an 8-element receiver array sensor prototype. The efficacy of both systems is evaluated empirically and through simulations.

Acknowledgments

Shahrzad Naghibzadeh
Delft, The Netherlands
July 16, 2014

Contents

List of Figures

List of Tables

1 Introduction

Smart office lighting systems exploit automated control of lighting and add flexibility by user-driven control to establish impressive energy savings while promoting user experience and occupants' comfort. In this thesis, we utilize an ultrasound-based smart antenna system for the design and implementation of a sensing system that provides granular occupancy information in a standard office room. Furthermore, we employ the same interface to provide a receiver for a communication system for user-driven light adjustment commands.

This chapter is dedicated to explaining the purpose and the significance of the schemes, the problems addressed and the main contributions. The chapter ends with describing the organization of the thesis.

1.1 Motivation

The design of energy-efficient lighting systems is important, given that electric lighting is a major constituent of electricity consumption in office buildings [3]. An approach to saving energy is by providing illumination at a given level only in occupied regions and providing lower illumination levels in unoccupied regions. Therefore, knowledge of occupant presence, movement flows and other spatio-temporal occupancy information is central to many smart building applications. Control schemes have been designed with these illumination objectives [4, 5]. A key ingredient in this approach is granular presence sensing, i.e., coarsely determining spatial occupancy in a given space. Furthermore, Granular presence and flow information may be used to provide occupancy analytics in buildings for improved facility management and optimization [6] and building emergency services [7]. While energy efficiency is an important design consideration, satisfaction of the individual user illumination needs and caring for users' comfort is equally important. Thus providing occupants with the ability to control lighting to meet individual needs is necessary. Control schemes may then take specific user inputs into consideration to enhance user satisfaction with the rendered illumination [8, 9].

A key factor that enables effective presence sensing systems is to exploit smart antenna configurations. One such configuration is the uniform circular array. This antenna comes with the major advantage of possessing a symmetrical configuration that provides for scanning the entire azimuth with slight change in the beam-width or the side-lobe level [10] since it has no edge elements [11]. Moreover, it can cover half elevation plane. Together with the range obtained from time-of-flight (ToF) of

a pulse-based radar system, these antennas can provide two-dimensional or three-dimensional target position when installed in a ceiling-mounted configuration.

Ultrasound signals possess a number of characteristics that make them a natural choice for room-based indoor localization purposes. The characteristics involve 1) negligible propagation through walls that guarantees zero interference between rooms, 2) low propagation velocity that makes them suitable for time-delay-based systems and 3) low cost of transducers [12]. Furthermore, speakers of the commodity mobile devices such as laptop or smart-phone are shown to be capable of producing inaudible sound frequencies up to 22 kHz [13, 14, 15]. Therefore, by employing a wide-band receiver we can integrate presence sensing and communication receiver functionalities into the same device and reduce hardware costs. Moreover, exploiting commodity mobile devices reduces the need for custom hardware such as remote controls or tags and further decreases hardware costs and adds to the user comfort.

1.2 Problem statement

The problem that we investigate in this thesis is twofold. One aspect of the problem is to design a real-time granular presence sensing system based on an ultrasonic uniform circular array receiver that can provide coarse-grained occupancy information inside a typical office room. The granular presence information is then passed to the lighting controller for providing pre-determined illumination levels in the occupied and unoccupied regions. The required accuracy of the system is in the order of human occupancy region which is about two square meters.

The second problem, considers exploiting the same receiver array to create a communication scheme through which individual occupants can transmit lighting control commands by using their laptop or smart-phone speakers without the need of any specialized hardware. Furthermore, the circular array receiver should specify the zone from which the user is transmitting the control command to apply the required adjustments in the specified zone. Here, the zone corresponds to the workspace of the occupant. By providing these information, the existing lighting control schemes are capable of adjusting the light level or other light features such as color in the specified region of the room accordingly.

1.3 Related work

Sensing systems for indoor positioning has received much attention in recent years. Many different techniques and algorithms exist for determining position of targets in the indoor environment. Liu et. al [16] present a comprehensive overview of these techniques. Some of these techniques are based on the use of different signal measurement methods to estimate the target position. These signal measurements

include Time Of Flight (TOF), Angle Of Arrival (AOA; also known as Direction Of Arrival (DOA)), and Received Signal Strength (RSS) to name a few. TOF is a method of measuring distance between the transmitter and the target by considering the fact that travelled distance is proportional to the propagation time of the signal. AOA method uses two or more antenna elements to estimate the angle from which the signal is reflected by means of the different received phase shifts of the transmitted signal at different antennas. RSS is based on the fact that the received signal strength drops as a function of distance and is based on path loss propagation model in a Line-Of-Sight (LOS) channel.

Moreover, different systems using different signal technologies exist for indoor localization [17]. Popular technologies for indoor applications include 1) Systems based on Radio Frequency (RF) which are further divided into narrow-band and wide-band systems. Among narrow-band systems technologies such as Radio Frequency Identification (e.g., [18]), Wireless Local Area Network (WLAN) [19] e.g., RADAR[20] and related technologies such as Bluetooth [21] and wireless sensor networks [22]. A popular RF-based wide-band system is the Ultra Wide-Band (UWB) system (e.g., [23]) which is the most fault-tolerant and accurate system for indoor localization among other RF-based systems. However the cost of UWB radars is high and all the RF-based signals can penetrate through walls and therefore are not appropriate for room-based systems. RF-based systems are usually combined with other technologies such as ultrasound [24] to provide room-level localization. 2) video-based systems such as the one discribed in [7] are intrusive, their non-intrusive counterpart that is based on computer vision techniques [25] suffer from sensitivity to varying lighting conditions in the room. 3) Systems based on Infra-Red (IR) (e.g., ActiveBadge[26]) are usually combined with other technologies to provide coarse-grained location estimate and are considered to show low detection sensitivity, 4) Systems based on ultrasound (e.g., [27, 28]) are relatively cheap and achieve fine-grained (centimeter-leve) indoor localization accuracy when combined with other technologies such as RF [29]. Most of the aforementioned systems are based on signal time delay measurement and require either a grid of sensors or that the user carry a tag at all times which in the latter case makes them intrusive.

Ultrasonic sensors are attractive for indoor presence detection for a number of reasons; (i)They can offer greater sensitivity over a larger detection region as compared to passive infrared sensors [30] at comparable costs. (ii) office rooms are isolated for sound and ultrasound has the same property of sound with higher frequency which makes it impossible to be detected outside the room and thus is appropriate for room-based applications and does not cause interference outside the room. (iii) The propagation speed of ultrasound in air is almost 6 order of magnitude lower than radio; This feature implies that an occupant moving even at a slow speed causes a much greater Doppler shift compared to radio. This makes them attractive for movement-based localization systems [31]. Apart from

ultrasonic positioning systems that provide room-based accuracy [24], ultrasonic systems are a popular technology among fine-grained (centemeter-level accuracy) Local Positioning Systems (LPS) e.g., Bat [28], Cricket [27], Dolphin [32] and [29] that are considered to provide robust location estimates with the accuracy of the order of centimeters. These systems combine ultrasound with RF and estimate TOF based on the slow propagation time of ultrasound and achieve a high accuracy in the range of few centimeters. The main drawbacks of these systems is that they require the user to carry a tag at all times, require LOS between the receiver/transmitter and the tags are very sensitive to background noise [33].

Indoor localization techniques have many applications ranging from robot navigation [34], human tracking [17], 3-D human computer interfaces [35], ubiquitous computing [36] and many more. One main application of indoor localization techniques is occupancy adaptive lighting control i.e., changing the lighting condition of the room based on occupancy information [37]. Continuous-wave Doppler ultrasonic sensors [38] are already used in these systems. In Doppler-based systems user presence is derived from induced Doppler frequency shifts and used to turn on or off the lighting system. However these Doppler ultrasonic sensors like passive infrared sensors only provide binary information on occupancy state. It is known that additional energy savings may be attained by exploiting granular occupancy information [39], [39]. Coarse-grained spatial occupancy can be used to achieve granular dimming in a lighting system [39] by adapting dimming levels of individual luminaries based on local occupancy conditions. In addition, such information may be used to create occupancy maps [40] and to analyze spatial movement patterns.

A pulsed-echo ultrasonic array sensor can provide range as well as angular information [41, 39, 42]. Ultrasonic linear array sensors were considered for localized presence sensing [41] in a wall-mounted configuration. Under a ceiling-mounted configuration, which is typical in indoor lighting control applications, these sensors were proposed for improved presence detection [39] and one-dimensional zoning [42]. With a linear array sensor in ceiling-mounted configuration, it is only possible to obtain information on the half-plane elevation angle. Furthermore, beams formed with uniform linear arrays, broaden significantly when the beam is steered away from the bore-sight [43]. A uniform circular array can, on the other hand, provide 360° azimuth angle as well as half-plane elevation angle information. Together with range, an occupant may thus be localized in a two-dimensional horizontal plane or the three-dimensional space based on the system requirement.

In addition, airborne ultrasonic sensors have been used for indoor communications [44, 45, 46, 47, 31, 48, 49]. In [47, 31], the feasibility of airborne ultrasonic communications at frequencies in the order of tens of kHz was investigated. In [50] propagation of ultrasonic signals including data (characters, images and voice) through air-filled and water-filled pipes was investigated. In [51] a simple PC mouse using narrow-band piezoelectric transducer with a center frequency of

40 kHz was designed using an analogue modulation scheme.In [44] OOK, BPSK, BFSK binary digital modulation schemes at the ultrasonic frequencies in range 200 to 300 kHz where tested on a polymer membrane transducer. The maximum bit rate achieved was 83 kbps at the maximum range of 2.8 meters. The LOS channel arrangement was established and the synchronization required for these schemes was performed through a physical link between the transmitter and the receiver. In [46] the same authors studied through-air communication of QPSK ultrasonic signals at the center frequency of 300 kHz and maximum signaling rate of 400 kbps using capacitive transducers. Maximum transmitter-receiver range obtained was 30 mm and LOS was assumed. In a later study, the same authors implemented a QPSK modulation scheme at the bit rate of 200 kbps. Capacitive transducers were used, LOS channel in the range of 1.2 m with a physical synchronization link between the transmitter and the receiver was established. In [49] DBPSK modulation implemented on a DSP board with dedicated ultrasonic transmitter and receiver was tested in a typical office environment. The transmission range was in the order of 4 m and LOS channel was obtained. In [48] a multi-channel OOK modulation scheme using capacitive transducers was designed to work at the bit rate of 60kbps and maximum LOS channel range of 0.6 m.

Moreover, It is shown that the speakers of the commercial off-the-shelf laptops and smart-phones are capable of producing ultrasound in the range of 20 kHz up to 22 kHz [13, 52, 14]. Produced ultrasonic signals do not show any audible noise as long as the speaker volume is kept bellow a threshold which is different for different brands of the speakers. The possibility of producing ultrasound on consumer laptops and smart-phones makes them a cheap and omnipresent platform for positioning as well as communication. Many researchers have used synchronized time-of-arrival with trilateration positioning technique to locate mobile phones [53, 14, 52, 54]. Moreover, acoustics and near-ultrasonic tones have been used as a means of Near-Field Communication (NFC) for short-range data transfer between mobile phones in the range of less than one meter [55, 15, 56]. In a resent work [57] an ultrasonic communication scheme using FSK at the frequencies 19.6 and 19.8 kHz was implemented and tested using commercial notebook computer speakers and microphones at the maximum LOS range of about 3 m. Similar schemes for near-ultrasonic communication using mobile phone speakers has been reported in [58, 59].

1.4 Contributions

In this thesis, we present an ultrasonic system based on the uniform circular receiver array geometry to provide the functionalities of granular presence sensing and user communication in a smart indoor lighting system. The first major contribution of our work is the real-time design of a granular presence sensing system to accurately locate the room occupants to the corresponding luminare coverage

region. This design is merely based on ultrasound and no additional technologies (such as RF) is used. Furthermore, unlike most fine-grained positioning systems, it is not intrusive in the sense that the user does not need to carry a tag.

The second major contribution of this thesis is the development of a real-time communication system to provide the room occupants with the means of sending lighting control commands. This system exploits the same wide-band uniform circular array receiver as the granular presence sensing system in a different frequency band and the existing speaker of the user's mobile phone or laptop for transmitting the command. The system, as mentioned earlier, does not require any additional hardware to perform the light remote controlling and by using the mobile phone or laptop speaker provides reliable communication throughout the room (maximum distance 6 m) given the LOS orientation of the speaker with the array receiver is maintained. Furthermore, the system is designed to provide the angular location of the user by means of 360 degrees azimuth angle scanning capability of the UCA receiver for applying the required changes in the corresponding region.

1.5 Outline

The thesis is organized as follows.

Chapter 2: Indoor granular presence sensing This chapter introduces the first contribution of the thesis which is the design of a granular presence sensing system for indoor occupancy location estimation and tracking. The chapter begins by describing the choice of the transmitted waveform, circular array geometry, applicable DOA estimation techniques, configuration of the room under test and the installation position of the transmitter-receiver pair. After the discussion of the practical design considerations, range estimation algorithm is presented. After the estimation of the range of the occupant, DOA processing algorithm is delineated to extract the occupant location. The observation points are then converted from spherical to Cartesian coordinates and supplied to the tracking algorithm described in the rest of the chapter to provide the filtered estimate of the target location. Moreover, a track scoring mechanism is provided for the purpose of distinguishing between occupant tracks and tracks due to persist-ant clutter and side-lobes.

Chapter 3: Combined control messaging and positioning This chapter details the second contribution of the thesis which is the design of a communication system between the room occupants and the receiver array for transmitting the lighting control commands. The chapter explains the major system components and design considerations of both the transmitter and the receiver, the effect of the ultrasonic channel is discussed on the transmitted waveform and the design constraints and assumptions are provided.

Chapter3: Experimental and simulation results In this chapter, the performance of the two systems is evaluated through experiments conducted in the test office. Moreover, simulations are performed to investigate the efficacy of the communication system under different indoor channel conditions. The results of the experiments as well as simulations are presented.

Chapter 5: Conclusion and future works This chapter concludes the thesis and gives some possible future directions for improving the proposed systems as well as some suggestions for future research in the area.

Indoor Granular Presence Sensing

2

In this chapter, the problem of indoor granular presence sensing for lighting control applications is addressed. We propose a presence sensing algorithm using an ultrasonic uniform circular array receiver and a co-located ultrasonic transmitter installed at the ceiling of a typical office room. To obtain coarse-grained occupancy information the transmitter sends pulsed sinusoid at regular pulse repetition intervals at a frequency that is within its bandwidth (for instance, commercial ultrasonic transducers used in building control applications have a typical center frequency of 40 kHz with a typical -6 dB bandwidth of 2 kHz). The circular array processes the received signal obtained after reflection from the objects in the environment. The preprocessed received signal is used to obtain granular presence information, which is then conveyed to the lighting controller for providing pre-determined illumination levels in the occupied and unoccupied regions.

To obtain granular presence information, the sampled raw received signal by the circular array is first preprocessed through a moving target indicator (MTI) processor to suppress static clutter. Afterwards, range information of potentially moving targets is extracted using a power detector applied to the down-mixed MTI-processed difference signal. A conventional beam-former [60] is then applied to the data in the ranges with detected movements to obtain azimuth and elevation angles with respect to the sensor. From the estimated range and angles of arrival, location estimates are obtained. These are converted to Cartesian coordinates, so that a linear tracker may be used. Thereafter, the detected observation points are supplied to the tracking algorithm. In order to distinguish true targets from clutter and false detections and account for potential missed detections, a two-dimensional Cartesian-coordinate tracking algorithm is proposed. The algorithm first associates measurements in each scan with tentative tracks based on a coarse gate [61] and a proximity-based clustering algorithm. The tracks are then filtered through a Kalman filter based on a near constant velocity (NCV) motion model[62]. To each tentative track, a score is assigned that consists of a signal-related term (SNR at the location), and a kinematic term (distance from the predicted location of the track from the previous scan). In order to confirm tentative tracks as true targets and delete tracks that have been lost for a number of scans, two corresponding thresholds are computed. Furthermore, for tracks in sufficiently close neighborhood, a track merger is applied that compares the state estimate of tracks and if for some number of scans the state estimates stay close, the redundant track is dropped.

2.1 System description

The presence sensing system consists of an 8-element circular array receiver with a co-located transmitter. The Ultrasonic transmitter used for presence sensing has a broad-beam pattern and a narrow bandwidth of about 2 kHz at -6 dB level (see Appendix1) with center frequency $f_{c,1} = 40$ kHz. The receiver array is made of M individual MEMS components that are sensitive to ultrasonic frequencies and their small size permits construction of a uniform circular array with limited spatial aliasing (the inter-element separation is close to half-wavelength, albeit higher, see Appendix 1). The sensor is located at the ceiling of a typical office room, a configuration that is common in indoor lighting control applications [4, 42]. We assume without loss of generality that the origin of the coordinate system is at the sensor. In this section we describe the transmitted waveform, circular array characteristics and the room configuration.

2.1.1 Transmitted waveform

In order to estimate the range of the occupant, TOF of the modulated pulses is used. There exist different waveforms for localization purposes with different range accuracies [63]. Since the required accuracy of this system is not higher than the dimensions of a human body, a pulsed sinusoid with appropriate pulse duration would suffice. The co-located transmitter with the receiver array sends out periodic pulsed sinusoid [41, 39], with an active transmission duration of T_s and pulse repetition interval being T_p. The transmitted signal can be written as a real-valued bandpass signal with center frequency $f_{c,1}$ as

$$s_1(t) = Re\{u(t)e^{j2\pi f_{c,1}t}\}, \quad 0 \leqslant t \leqslant T_p,$$

where $Re\{.\}$ represents the real part, and

$$u(t) = \begin{cases} 1 & 0 < t - \lfloor \frac{t}{T_p} \rfloor T_p \leqslant T_s \\ 0 & T_s < t - \lfloor \frac{t}{T_p} \rfloor T_p \leqslant T_p \ . \end{cases}$$

To perform MTI processing on the received echos when estimating the range of the moving occupants, two consecutive pulses are used. In the rest of the chapter, two pulse repetition intervals constitute a scan as depicted in Fig 2.1

2.1.2 Circular array sensor and beam-forming methods

The receiver is a circular array with M elements uniformly distributed on a circle with radius r as shown in Fig 2.2. The receiver is broadband, capable of covering wide range of ultrasonic frequencies (see Appendix 1). For presence sensing purposes, the receiver is tuned to the central frequency of the ultrasonic transmitter ($f_{c,1}$). This is while for the reception of the control messaging (explained in

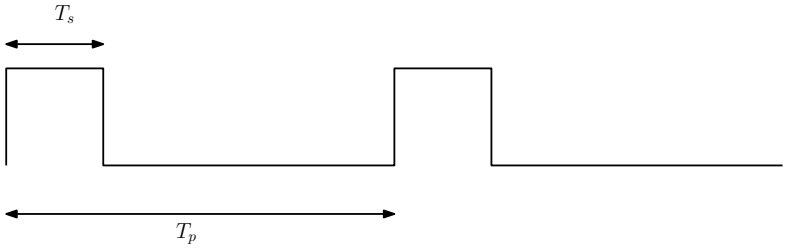

Figure 2.1: Transmitted pulses contained in a scan.

Chapter 3), the receiver is tuned to to the central frequency of the mobile devices ($f_{c,2}$). A spherical coordinate system with origin at the center of the receiver is considered for direction of arrival (DOA) estimation of the back-scattered plane waves. Elevation angles in the range $\theta \in [0, \pi/2]$ are measured with respect to the positive direction of the z-axis, which in our case is directed from the ceiling towards the floor. Azimuth angles of the impinging plane waves are in the range of $\phi \in [0, 2\pi)$ and are measured counterclockwise from the x-axis in the $x - y$ plane of the ceiling as depicted in Fig 2.2. Assuming the alignment of the first array

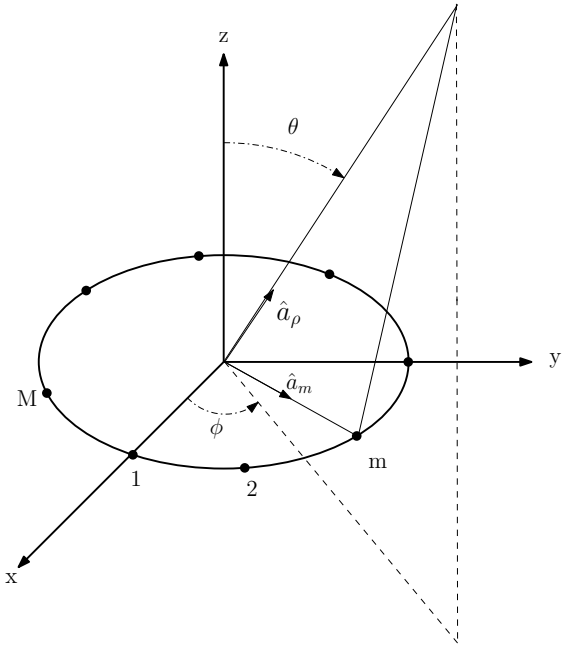

Figure 2.2: Impinging planar wave and the geometry of a uniform circular array with M equally-spaced elements.

element with the positive direction of the x-axis, the angular position of the array

elements [64, 10]

$$\phi_m = 2\pi\left(\frac{m-1}{M}\right),\ m = 1, 2, ..., M,$$

A narrow-band planar waves with wavelength $\lambda = v_s/f_{c,1}$ that impinges on the array form the elevation angle θ and the azimuth angle ϕ. The difference in the distance by which the planar wave reaches the mth element with respect to the origin of the array is given in [64] as $r\cos\Psi_m$. For incoming waves, as shown in Fig 2.2 $\cos\Psi_m$ equals

$$\begin{aligned}
&\cos\Psi_m = -\hat{a}_\rho \cdot \hat{a}_m \\
&= -(\hat{a}_x \sin\theta\cos\phi + \hat{a}_y \sin\theta\sin\phi + \hat{a}_z\cos\theta)\cdot(\hat{a}_x\cos\phi_m + \hat{a}_y\sin\phi_m) \\
&= \sin\theta\cos(\phi - \phi_m)
\end{aligned}$$

Were $\hat{a}_\rho$ and $\hat{a}_m$ respectively denote the unit vector from the origin of the array to the observation point and the unit vector from the origin to the mth element of the array. Therefore, the relative delay in the reception of the wavefront with respect to the origin of the array are respectively given by

$$\tau_m = -\frac{r}{v_s}\sin(\theta)\cos(\phi - \phi_m),\ m = 1, 2, ..., M. \tag{2.1}$$

Consequently, the element-space circular array response is given by the steering vector:

$$\boldsymbol{a}(\theta,\phi) = \begin{pmatrix} e^{j\frac{2\pi}{\lambda}r\sin\theta\cos(\phi-\phi_1)} \\ e^{j\frac{2\pi}{\lambda}r\sin\theta\cos(\phi-\phi_2)} \\ \vdots \\ e^{j\frac{2\pi}{\lambda}r\sin\theta\cos(\phi-\phi_M)} \end{pmatrix}, \tag{2.2}$$

In order to investigate the beam-pattern of the circular array at the operating frequency of $f_{c,1} = 40$ kHz, the spatial response of the array to the $\underline{1}_{(M\times 1)}$ beamformer is applied to the array response vector. Where $\underline{1}_{(M\times 1)}$ denote the vector of length M with all one entries.The spatial pattern is calculated as

$$|\underline{1}^T_{(M\times 1)}\boldsymbol{a}(\theta,\phi)|$$

for elevation and azimuth angle varying in the range $\theta \in [0, \pi/2]$ and $\phi \in [0, 2\pi)$ respectively. The result is shown in Fig 2.3 . As can be seen, apart from the main beam, due to the fact that the inter-element spacing Δm is slightly greater than $\lambda_1/2$, side-lobes appear at the elevation angle of about 50 degrees as depicted in Fig 2.3(b). As is plainly evident from the picture, UCA possesses a periodic beam-pattern in azimuth [11].

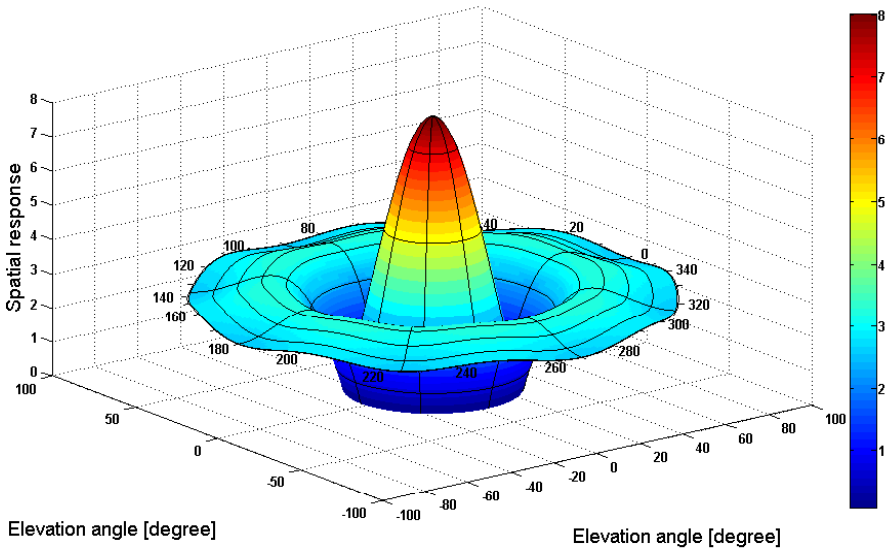

(a)

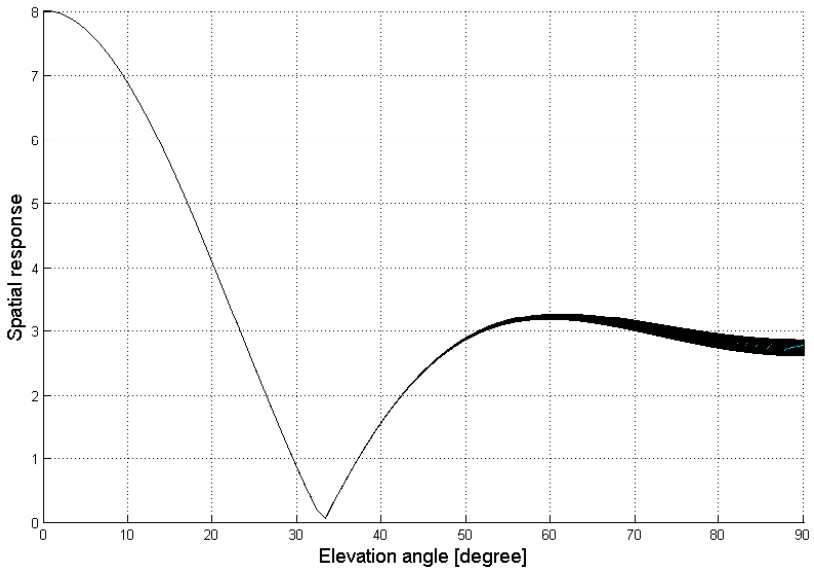

(b)

Figure 2.3: (a) Spatial response of the UCA at 40 kHz. ,(b) Spatial response of the UCA at 40 kHz versus elevation angle.

2.1.2.1 Applicable DOA estimation algorithms to the Uniform Circular array

In order to estimate the direction from which the source signals are impinging on the array and to locate the source in the angular domain, it is necessary to apply direction finding algorithms. However, most direction finding algorithms have been originally designed for the uniform linear array (ULA) and are not directly applicable for the UCA. Tan et.al [11] have reviewed the direction-finding methods that are applicable on the UCA. In the sequel, we investigate some of these methods together with their pros ans cons to justify the beam-forming choice for our system. Let us assume K sources are impinging on the circular array with M elements. The Received signal by the M antennas can be expressed as [60]

$$\boldsymbol{x}(t) = \boldsymbol{A}\boldsymbol{s}(t) + \boldsymbol{n}(t)$$

where $\boldsymbol{x}(t)$ is an $M \times 1$ vector of received signal from the M antenna elements, $\boldsymbol{n}(t)$ is the $M \times 1$ vector of receiver noise per antenna element and $\boldsymbol{A}(t)$ and $\boldsymbol{s}(t)$ are the $M \times K$ array response matrix and $K \times 1$ source vector respectively as

$$\boldsymbol{s}(t) = [s_1(t), \ldots, s_K(t)]^T,$$

$$\boldsymbol{A}(t) = [a(\theta_1, \phi_1), \ldots, a(\theta_K, \phi_K)]$$

where $a(\theta, \phi)$ is the array response vector defined in equation 2.2. Assuming that source and noise vector are uncorrelated and different antenna elements have mutually uncorrelated noise with variance σ_n^2, The spatial correlation matrix of the sampled-time received signal can be expressed as

$$\boldsymbol{R}_x = \boldsymbol{A}\boldsymbol{R}_{\boldsymbol{s}}\boldsymbol{A}^H + \sigma_m^2\boldsymbol{I}_M$$

Where $\boldsymbol{R}_s = E[\boldsymbol{s}(t)\boldsymbol{s}^H(t)]$ and $E[\boldsymbol{n}(t)\boldsymbol{n}^H(t)] = \sigma_m^2\boldsymbol{I}_M$ are respectively the source and noise correlation matrix and $\boldsymbol{I}_M$ denotes $M \times M$ identity matrix. When the incoming sources are uncorrelated, the signal correlation matrix $\boldsymbol{R}_{\boldsymbol{s}}$ is full rank and diagonal. However, if the incoming signals are correlated, $\boldsymbol{R}_{\boldsymbol{s}}$ is rank deficient and non-diagonal [65].

In the case of the propagation of the ultrasound signal in the indoor environment, due to multi-path propagation, signals reflected from different parts of the occupant body form correlated incoming source signals at the receiver. By applying DOA estimation algorithms on these signals, we are able to discover the elevation and azimuth angle from which the occupant signals are arriving to the array. Taking into consideration 1) the array geometry, 2) indoor multi-path propagation environment 3) existence of multiple point sources reflecting the signal in the occupant body 4) limited computational capacity and real-time system requirements, we have chosen the classical beam-former among the existing beam-forming and high resolution DOA estimation techniques applicable on the UCA. In the following paragraphs we justify our choice by briefly introducing the applicable beam-forming methods for the UCA.

DOA estimators applicable to arbitrary array geometries

1. Conventional beam-former

   The conventional beam-former takes the array response vector as beamforming weight and by computing the spatial spectrum, looks for the location with the maximum received power which corresponds to the source location[60]. The beam-forming weights and the corresponding spatial spectrum are denoted respectively as

$$\boldsymbol{w}_{conv} = \boldsymbol{a}(\theta, \phi)$$

$$\boldsymbol{\Lambda}_{conv}(\theta, \phi) = \frac{\boldsymbol{a}^H(\theta, \phi)\boldsymbol{R}_x\boldsymbol{a}(\theta, \phi)}{\boldsymbol{a}^H(\theta, \phi)\boldsymbol{a}(\theta, \phi)}$$

   where $\boldsymbol{w}_{conv}$ and $\boldsymbol{\Lambda}_{conv}(\theta, \phi)$ respectively denote the conventional beamformer weight vector and spatial spectrum. DOA estimation consists of a 2 dimensional search in the spatial spectrum. Therefore, the major computational requirement for this method is a 2D spectrum search. The consistency of this method degrades as the number of sources increase to more than one source. An example of the conventional beam-former spatial spectrum achieved from our 8-element array at 40 kHz for a single source is shown in Fig 2.4.

2. 2D-MVDR

   The MVDR beam-former weight vector is obtained from minimizing the output power of the beamformer while constraining the power at the desired direction to one [60]. This method produces weight vector and spacial spectrum respectively expressed as

$$\boldsymbol{w}_{MVDR} = \frac{R_x^{-1}\boldsymbol{a}(\theta, \phi)}{\boldsymbol{a}^H(\theta, \phi)R_x^{-1}\boldsymbol{a}(\theta, \phi)}$$

$$\boldsymbol{\Lambda}_{MVDR}(\theta, \phi) = \frac{1}{\boldsymbol{a}^H(\theta, \phi)R_x^{-1}\boldsymbol{a}(\theta, \phi)}$$

   where $\boldsymbol{w}_{MVDR}$ and $\boldsymbol{\Lambda}_{MVDR}(\theta, \phi)$ respectively denote the MVDR weight vector and spatial spectrum. To determine the source direction, a 2D spectral search is required. Therefore the major computational requirements are matrix inversion and 2D spectral search. It was shown through experiments that the added complexity of matrix inversion (even by applying the Levinson algorithm [66]) violated the real-time requirement of our presence sensing system. An example of the MVDR spectrum applied to the array response of an 8-element uniform circular array for a single source at 40 kHz is shown in Fig 2.5.

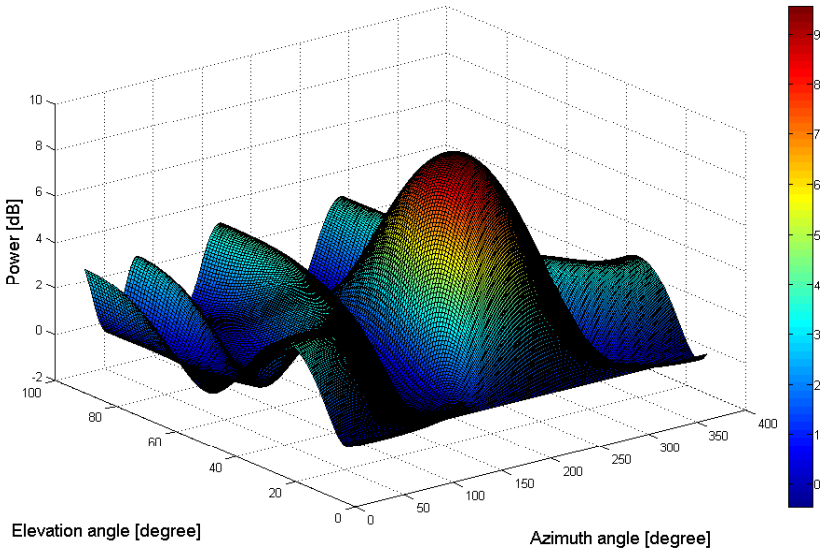

(a)

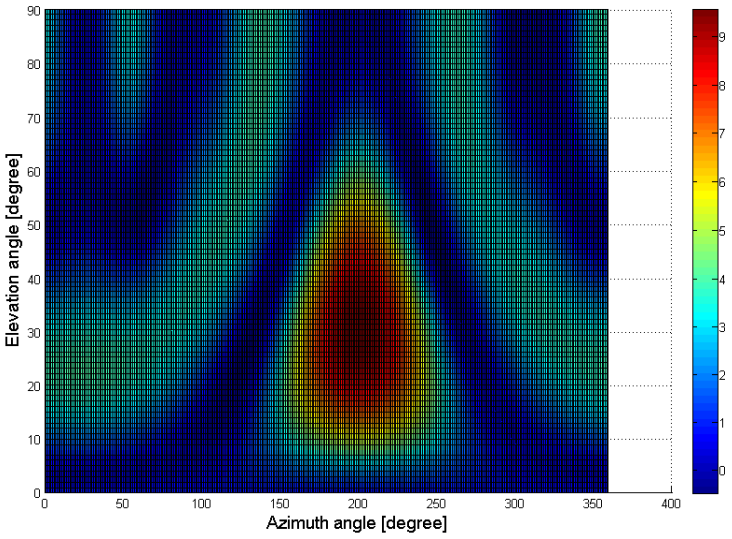

(b)

Figure 2.4: (a) Result of the conventional beam-former for a source at $\theta = 30^\circ$ and $\phi = 200^\circ$, $SNR = 20$ dB. ,(b) Top view.

3. 2D-MUSIC

The MUSIC algorithm is based on the eigenvalue decomposition of the

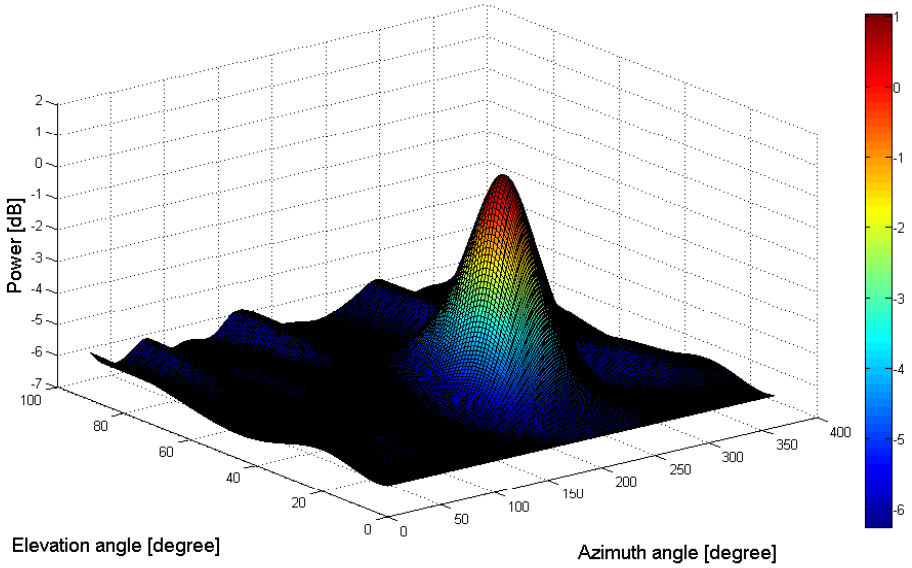

(a)

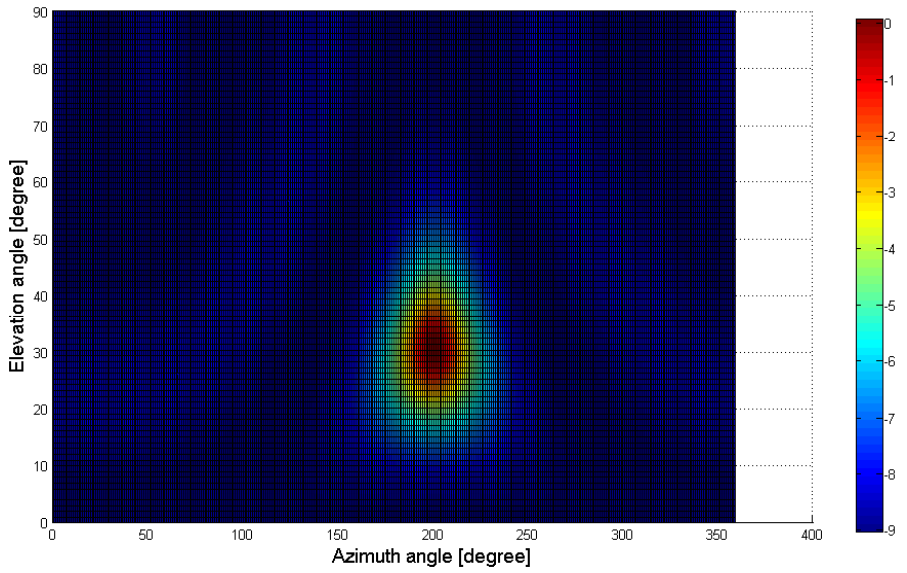

(b)

Figure 2.5: (a) Result of the MVDR beam-former for a source at $\theta = 30^\circ$ and $\phi = 200^\circ$, $SNR = 20$ dB. ,(b) Top view.

covariance matrix $\boldsymbol{R}_x$ and the orthogonality of the noise subspace to the array response vector. MUSIC algorithm gives rise to the spatial spectrum

expressed as

$$\mathbf{\Lambda}_{MUSIC}(\theta,\phi) = \frac{\boldsymbol{a}^H(\theta,\phi)\boldsymbol{a}(\theta,\phi)}{\boldsymbol{a}^H(\theta,\phi)U_n U_n^H \boldsymbol{a}(\theta,\phi)}$$

where $\mathbf{\Lambda}_{MUSIC}$ is the MUSIC spatial spectrum and U_n denotes the noise eigenvector. The major computations in this method consist of eigenvalue decomposition and 2D spectral search. The added eigenvalue decomposition is computationally expensive for our system and violates the real-time requirements. Furthermore, in the multi-path environment of our test office, since the incoming sources are coherent and matrix R_x is rank deficient, spatial smoothing must be applied prior to eigenvalue decomposition. However, The spatial smoothing method is based on the Vandermonde structure in the uniform linear array and is not directly applicable to the UCA. In the following paragraph, phase mode excitation-based beam-formers are briefly introduced. By applying the beam-space transform [67] to the UCA array response a similar structure as the Vandermonde structure of the ULA is obtained.

phase-mode excitation-based beam-forming methods As has mentioned in Section 2.1.2, UCA has a periodic beam-pattern in azimuth. By using Fourier analysis, the beam-pattern can be decomposed into different Fourier harmonics [11]. Phase-mode excitation is referred to each of these Fourier harmonics [68]. By applying the phase-mode excitation to UCA array response vector, a phase-mode steering vector possessing the Vandermonde structure similar to the ULA array response vector is attained. UCA Real Beam-space MUSIC (UCA-RB-MUSIC) and UCA-ESPRIT are two high resolution DOA estimation methods based on the phase-mode excitation principal [67]. The phase-mode array response consists of at most M' elements where $M' \leqslant M/2$. Therefore the number of sources that can be resolved is $M' - 1$ which is less than half of the antenna elements. Therefore, the Vandermonde structure is attained through phase mode excitation at the cost of loosing half of the antenna elements. Other novel methods such as the sparse ruler [69] can be applied on the phase-mode array response of the UCA to increase the number of resolvable sources. The methods based on the phase-mode excitation are computationally expensive to be implemented in our real-time system, furthermore, the decreased size of the array response restricts the number of occupants that can be detected in the room.

2.1.3 Room configuration and sensor installation

The transmitter and the co-located receiver (shown in Fig 2.6) are installed in approximately the center of the ceiling of an office room of height $\hat{h}$, width $\hat{w}$ and length $\hat{l}$ as depicted in Fig 2.7. The transmitted signal power is adjusted as such to cover the maximum coverage range of R_{max} as shown in Fig 2.7.

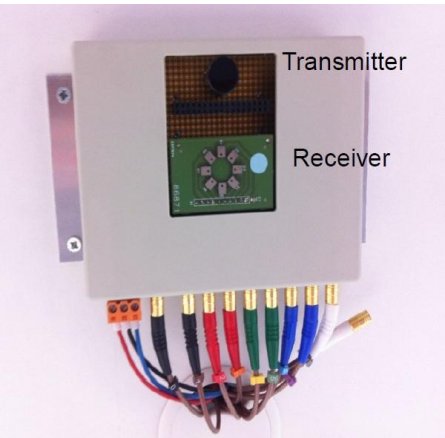

Figure 2.6: Sensor prototype at ceiling.

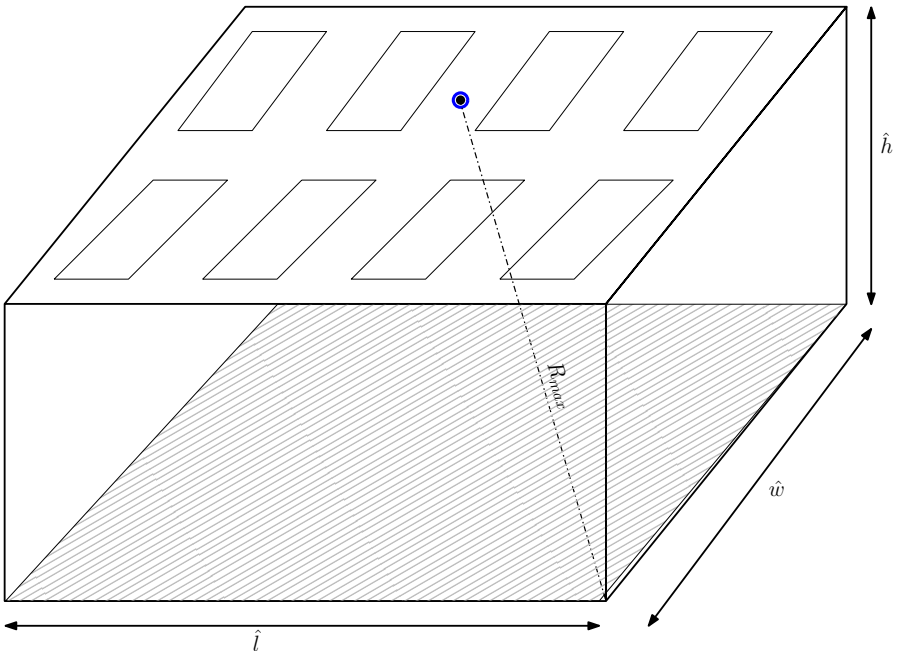

Figure 2.7: Sensor prototype at ceiling.

2.1.4 Propagation of the ultrasound in the indoor environment

Multi-path and clutter As the ultrasound signal propagates in the indoor environment, it experiences a number of challenges. First, the ultrasound signal is reflected from rigid objects and walls. If the reflected signal reaches the receiver, it causes multi-path in the received signal. Multi-path echoes experience a longer path duration than the LOS echoes. Therefore, in a room-based system, a num-

ber of the locations estimated due to the multi-path echoes can be disregarded by applying room-level filtering. The back-scattered signal echoes from the unwanted objects is called clutter. As the ultrasound signal hits the sharp edges of the furniture or other objects in the indoor environment, it is scattered, causing a number of unwanted echoes in the received signal [70].

Reverberation Ultrasound continues to remain in a room once the source has terminated producing it. This phenomena is called reverberation in the acoustic literature. Due to the path loss, the ultrasound signal strength reduces with the traveled distance. Moreover, by reflecting from objects inside the room, ultrasound signal level drops due to absorption from the objects. The time required for the strength of the reflected ultrasound rays to drop bellow 60 dB from the LOS path sound ray is called reverberation time (RT) [31]. The -60dB point is a conservative criterion. Typical values of the reverberation time in the indoor environment are $50 - 300$ ms.

Noise There is a large variation in the background noise level experienced by the ultrasound. The variation is about 50 dB [31]. In a study conducted in an industrial environment, a background noise level of $70 - 80$ dB sound pressure level (SPL) was reported [71].

Doppler shift Due to the slow propagation speed of the ultrasound in air as compare to RF, reflections from a moving object are received with a higher Doppler shift. The frequency shift of the moving objects with the radial speed v_r at the operating frequency f_0 is calculated as

$$f_d = \pm \frac{f_0 v_r}{v_s}$$

where v_s is the speed of sound in air and f_d is the Doppler frequency shift. Since the speed of sound is much lower than the speed of light, it causes a greater Doppler shift. Therefore, ultrasound is a better choice for movement-based localization systems than RF.

2.2 Receiver signal processing

Ultrasonic environment is a challenging environment that causes a number of complications to the propagation of the ultrasound signal in the indoor environment. These challenges include noise, reverberation and Doppler shift [47] as previously mentioned. The receiver uses digital signal processing to cope with these issues as well as to extract required information from the received signal. This section describes the signal processing applied to the raw received signal to estimate the

occupant location and form the measurements to supply to the tracker. As shown through the block diagram in Fig 2.8, first, the received signal is demodulated and converted to base-band. Then, MTI processing is applied to suppress the effect of static clutter. Subsequently, range values corresponding to possible occupant movements are estimated by applying a power detector on the clutter-suppressed difference signal. In the next step, data from the tentative target range is provided to a beam-former to extract azimuth and elevation angles of arrival. Thereafter, the measured locations in spherical coordinates are converted to Cartesian coordinates and used as input to the tracker.

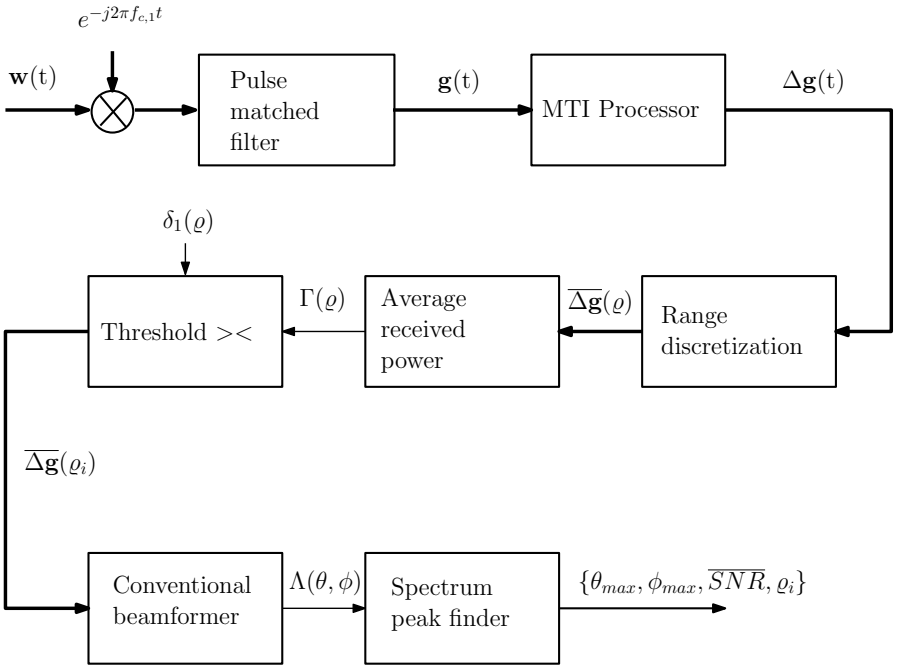

Figure 2.8: Presence sensing receiver block diagram.

2.2.1 Conversion to base-band

The received signal at the receiver elements is a real-valued bandpass signal represented as

$$w_m(t) = Re\{g_m(t)e^{j2\pi f_{c,1}t}\}$$

where $w_m(t)$ is the received signal at the mth element and $g_m(t)$ represents the complex envelope of the received signal. Due to multi-path caused by static and moving clutter in the indoor environment, the sinusoidal pulse is received from multiple paths with different attenuation, delay and Doppler shift and it is the sum of multiple such echoes.

In order to down-convert the received signal to base-band, the received signal is multiplied with the complex exponential $e^{-j2\pi f_c t}$ [72] and a low-pass filter is applied with cut-off frequency $f_{D,max}$ to allow for Doppler shifts.

2.2.2 Moving target indicator processing

We apply single canceller MTI processing [72], based on the subtraction of echoes received over two consecutive pulse intervals (called a scan), to suppress the effect of the static clutter. More specifically, the base-band received signal at the mth element at time instant t with respect to the beginning of the pulse is composed of $N(t)$ components and can be expressed as

$$g_m(t) = \sum_{n=1}^{N(t)} \beta_{m,n}(t) u(t - T_{m,n}(t)) e^{-j2\pi f_{c,1} T_{m,n}(t)} e^{j2\pi f_{D_{m,n}}(t)} + \zeta_m(t) \tag{2.3}$$

where $N(t) = N_1(t) + N_2$ is composed of $N_1(t)$ components due to moving clutter and N_2 components due to static clutter, $\beta_{m,n}(t)$ denotes the complex attenuation factor of the nth path

$$\beta_{m,n}(t) = \hat{\alpha}_{m,n}(t) e^{-j2\pi f_{c,1} T_{m,n}(t)}$$

where $\hat{\alpha}_{m,n}$ denotes attenuation gain and $T_{m,n}(t)$ denotes time delay of the nth path with respect to the mth receiver element at time t. The nth resolvable multi-path component may be due to one scatterer or a cluster of nearby scatterers having similar delays. $\zeta_m(t)$ is the additive white Gaussian noise at the mth element. We assume that the noise on different antenna elements are uncorrelated. The terms $T_{m,n}(t)$ and $f_{D_{m,n}}(t)$ are respectively the time delay and Doppler shift of the nth path at time t and are given by

$$T_{m,n}(t) = \frac{2d_{m,n}(t)}{v_s}, \; f_{D_{m,n}}(t) \approx \frac{2v_{m,n}(t)}{\lambda},$$

where $d_{m,n}(t)$ is the nth path length with respect to the mth antenna element and $v_{m,n}(t)$ is the radial speed of the object that has caused the echoes with respect to the mth antenna element.

The MTI processor subtracts the echo received at a time instant t from the corresponding echo received at the next pulse repetition interval. That is, for the mth element,

$$\Delta g_m(t) = g_m(t + T_p) - g_m(t).$$

For echoes caused by static objects, the Doppler frequency is zero, and since path length and therefore delay does not change over time, the difference signal after MTI processing due to received signals from static objects is zero. Therefore, the difference signal only contains $N_1(t)$ components. Assuming that the number

of moving multi-path components and the speed of the objects caused by each component is constant over a scan, that is

$$N_1(t+T_p) = N_1(t) = N_1,$$
$$f_{D_{m,n}}(t) \approx f_{D_{m,n}}(t+T_p) = f_{D_{m,n}},$$

the output of the MTI processor can be written as

$$\begin{aligned}\Delta g_m(t) &= e^{j2\pi f_{D_{m,n}}}\Big(\sum_{n=1}^{N_1}\beta_{m,n}(t+T_p) - \sum_{n=1}^{N_1}\beta_{m,n}(t)\Big) \\ &\quad +\zeta_m(t+T_p) - \zeta_m(t).\end{aligned}$$

Therefore, the gain difference of the nth echo component, $\beta_{m,n}(t+T_n) - \beta_{m,n}(t)$, can be zero for certain blind speeds [41] when the gain difference

$$\beta_{m,n}(t+T_p) - \beta_{m,n}(t) = \hat{\alpha}_{m,n}[e^{\frac{-j4\pi d_{m,n}(t+T_p)}{\lambda_1}} - e^{\frac{-j4\pi d_{m,n}(t)}{\lambda_1}}], \tag{2.4}$$

is zero. Furthermore, since the distnace of the travelled distance of the incomming signal is much greater than the radius of the array, we can approximate

$$d_{m,n}(t) \gg r \Rightarrow d_{m,n}(t) \approx d_n(t),\ v_{m,n}(t) \approx v_n(t)$$

where $d_n(t)$ and $v_n(t)$ are respectively the travelled distance and radial speed of the nth multipath component with respect to the center of the array. To find the blind speed, the term in brackets in equation 2.4 can be further expressed as

$$\begin{aligned}&e^{\frac{-j4\pi d_n(t+T_p)}{\lambda_1}} - e^{\frac{-j4\pi d_n(t)}{\lambda_1}} \\ &= e^{\frac{-j4\pi d_n(t)}{\lambda_1}}[e^{-j4\pi\frac{d_n(t+T_p)-d_n(t)}{\lambda_1}} - 1] \\ &= e^{\frac{-j4\pi d_n(t)}{\lambda_1}}[e^{-j4\pi\frac{v_n(t)T_p}{\lambda_1}} - 1]\end{aligned}$$

Therefore, zero gain is obtained when

$$4\pi\frac{v_n(t)T_p}{\lambda_1} = 2\pi$$

This gives the expression for the radial speed of the occupant for which the MTI processor suppresses the received echo. The blind speed v_{blind} is denoted as

$$v_{blind} = \frac{\lambda_1}{2T_p}$$

The effect of the suppression caused by MTI processor is the discontinuous detection of the occupant if the radial speed at some point equals the blind speed. This signifies the need for tracking so as not to lose track of the occupant movements.

2.2.3 Range processing

To detect the location of the occupants in the office room, we first extract range information from the received echo. For the purpose of practical implementation, we discretize the range covered over a scan duration into a number of range bins. The size of the range bins will determine the range measurement granularity of our system. We choose the size of each range bin to be $\Delta d = 0.343$ m; Therefore, the range accuracy of our system is half of the range resolution ΔR. The ϱth range bin is denoted as

$$d(\varrho) = (\varrho - 1)\Delta d, \;\; \varrho = 1, 2, ..., \frac{R_{max}}{\Delta d}.$$

Since the signal is digitized at the receiver with sampling frequency $f_{s,1}$, the ϱth range bin contains $\nu = \lfloor \frac{2\Delta d f_{s,1}}{v_s} \rfloor$ samples. The received samples in one range bin are summed. This summation implements a moving average filter that performs low-pass filtering on the received echos. The result of the moving average filtering on the MTI-processed received data for individual antenna elements is shown in Fig 2.9.

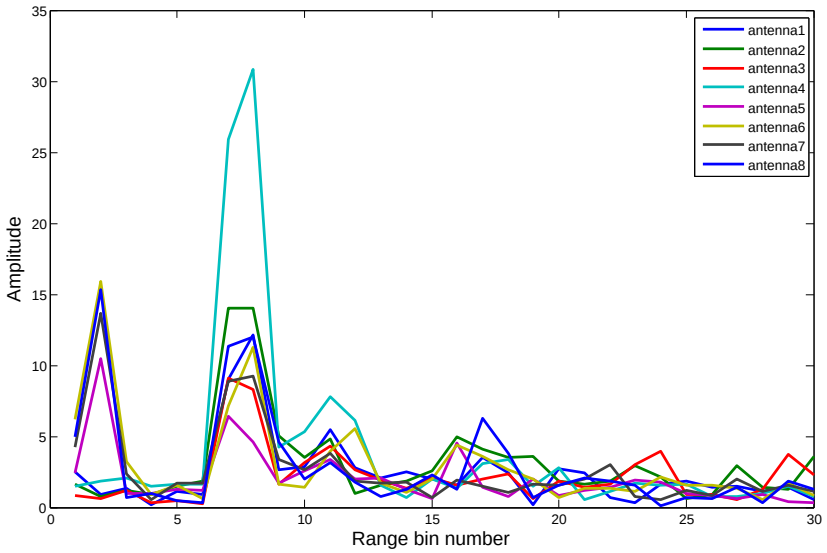

Figure 2.9: Base-band received signal over different antenna elements.

Due to electromagnetic coupling between antenna elements, a portion of the received signal corresponding roughly to 3 range bins are influenced and therefore are discarded in the further processing steps. Furthermore, the range bins corre-

sponding to the increased listening time within pulses for reverberation subsidence, are discarded.

Let the down-mixed and MTI-processed portion of the received signal at the mth array element for sample ς at the ϱth range bin be denoted as $\overline{\Delta g}_m(\varrho,\varsigma),\ \varsigma = 1,2,...,\nu$. The preprocessed signal at the ϱth range bin for ςth sample received by M elements is given by

$$\overline{\boldsymbol{\Delta g}}(\varrho,\varsigma) = \left[\overline{\Delta g}_1(\varrho,\varsigma), \overline{\Delta g}_2(\varrho,\varsigma), \ldots, \overline{\Delta g}_M(\varrho,\varsigma)\right]^T.$$

To detect movement, the average received power per range bin received over all the elements is computed as

$$\Gamma(\varrho) = \frac{1}{M\nu}\sum_{m=1}^{M}\sum_{\varsigma=1}^{\nu}|\overline{\Delta g}_m(\varrho,\varsigma)|^2.$$

The power per range bin is then compared against a threshold. The detection threshold $\delta_1(\varrho)$ per range bin ϱ is set using the noise power, $\epsilon(\varrho)$, measured when the environment is unoccupied, so as to achieve a desired probability of false alarm (we choose a value of $P_{FA} = 10^{-3}$). To compute threshold the receiver noise power is collected at multiple sessions when the room was unoccupied and the histogram was calculated per each range bin as shown in Fig 2.10. As can be seen the this figure and as already mentioned earlier, the first three range bins have much higher received power due to the electromagnetic coupling between antennas and are thus discarded from further processing steps. The corresponding threshold per range bin is shown in Fig 2.11. Due to multi-path propagation in the indoor environment, echoes from the same moving occupant reach the receiver with different delays in multiple range bins after power detection. We consider that the strongest echo is due to the line-of-sight component between the closest occupant and the sensor. In order to deal with the effect of multi-path and since the number of occupants is not known a priori, we consider the following processing steps. First, the range bin with the maximum received power is chosen and compared against the corresponding detection threshold as illustrated in Fig 2.12 for one pulse scan. Let ϱ_{max} denote the range bin with the maximum received power. If the following condition holds,

$$\Gamma(\varrho_{max}) > \delta_1(\varrho_{max}),$$

we conclude that the room is occupied. Thereafter, all other range bins with received power higher than or equal to $\frac{\Gamma(\varrho_{max})}{4}$ are compared against their corresponding detection threshold. More specifically, if for the ϱth range bin the following condition holds,

$$\Gamma(\varrho) \geqslant \max\{\delta_1(\varrho), \frac{\Gamma(\varrho_{max})}{4}\},$$

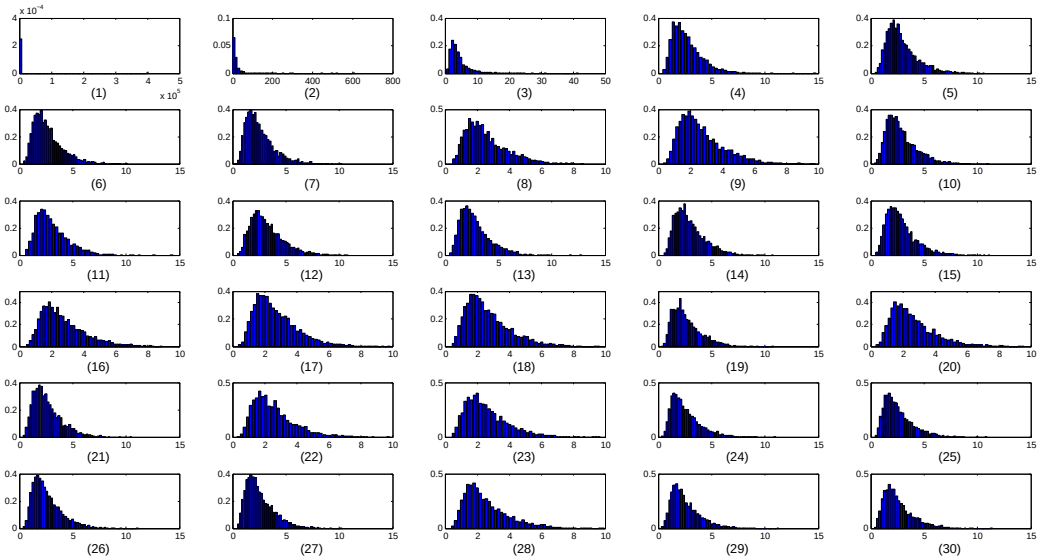

Figure 2.10: Noise histogram per range bin.

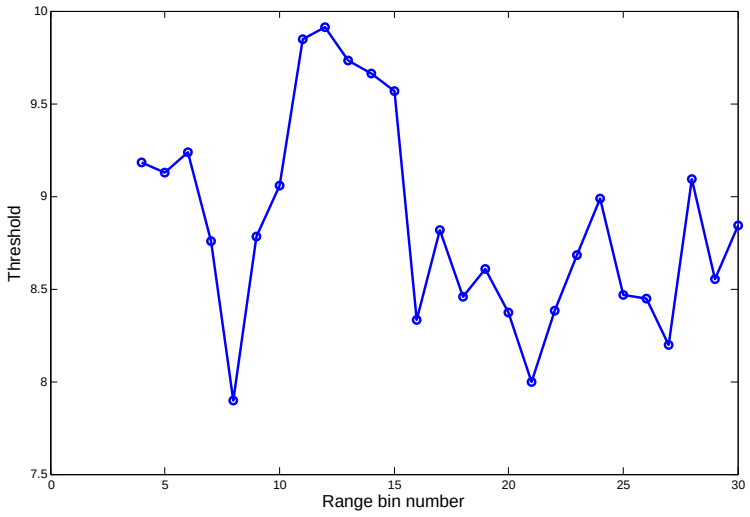

Figure 2.11: Detection threshold per range bin.

then that range bin is declared as a possible range bin where an occupant is located and considered for further processing. This procedure may still allow multi-path echoes to be declared as active range bins. The tracking algorithm is designed to correct some of these false detections.

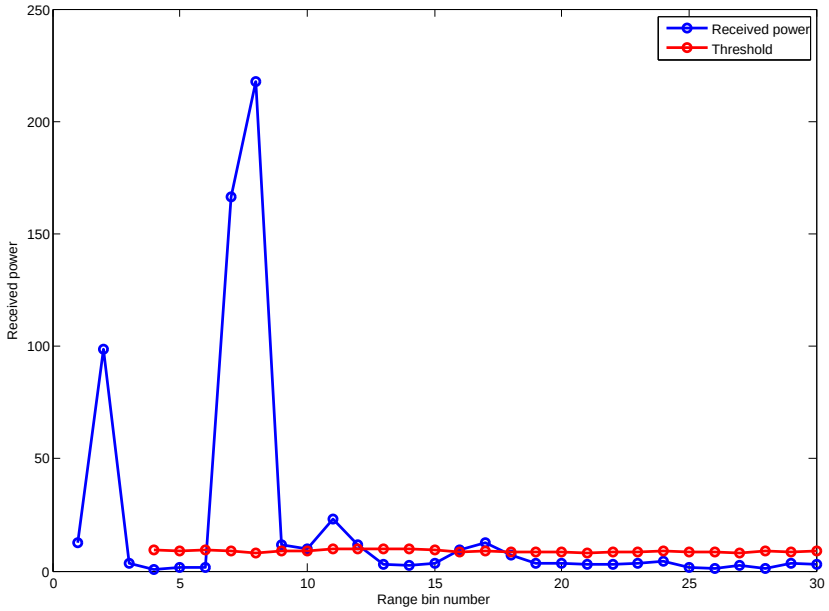

Figure 2.12: Received power in one scan compared with the threshold.

2.3 Practical design considerations

The target detection area that the sensor should achieve is 40-50 m^2, at a mounting height of 2.5-3 m, considering typical topologies of cellular offices and zones in open offices. As an example, the office space considered in our experiments has a length of $\hat{l}$ =7.6 m and width $\hat{w}$ =6 m, with the sensor mounted on the ceiling at a height of about $\hat{h}$ =3 m, at roughly the center of the room. The maximum range to be covered by the sensor is then

$$R_{max} = \sqrt{\hat{l}^2 + \hat{w}^2 + \hat{h}^2} \approx 6\ m.$$

Considering the speed of sound in air to be $v_s = 343\ \mathrm{ms}^{-1}$ and given the center frequency of the transmitted narrow-band waveform is $f_{c,1} = 40$ kHz, the wavelength λ_1 is

$$\lambda_1 = \frac{v_s}{f_{c,1}} \approx 8.6\ mm.$$

We considered an 8-element uniform circular array so as to have a reasonable spatial granularity while keeping the sensor complexity low. Due to the size of available commercial components used to construct the receiver array, the inter-element spacing is Δm = 4.614 mm. Since this value is slightly higher than the

half-wavelength, we expect to have some spatial aliasing in the form of spatial side-lobes in the beam pattern. This needs to be alleviated in the receiver processing so as to avoid falsely detecting non-existent occupants. The circular array dimensions are shown in Fig 2.13.

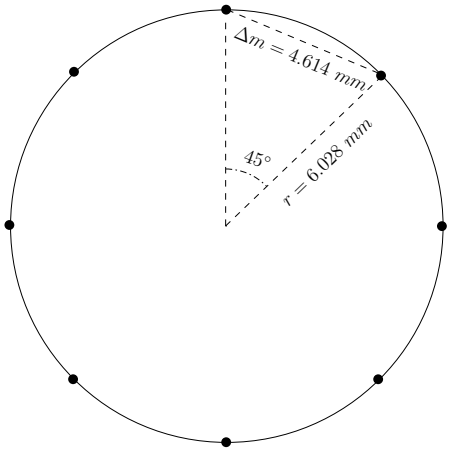

Figure 2.13: Array sensor dimensions.

In order to treat spherical wave-fronts as plane waves, a user is required to be in the far field of the array sensor [64]. Given that the circular array has a radius $r \approx 6$ mm, and with a mounting height of 3 m, the far field conditions are satisfied [64].

To satisfy far field condition, three terms must be met [64]

$$R \gg D,\ R \gg \lambda_1,\ R \gg \frac{2D^2}{\lambda_1}$$

where R is the distance of the source from the array and D is the maximal distance across the antenna array– the aperture. In our system, circular array has a radius of $r \approx 6$ mm; Therefore the aperture is $D \approx 12$ mm. To satisfy the conditions, distance of the source should be respectively greater than:

$$R \gg 12\ mm,\ R \gg 8.6\ mm,\ R \gg 33.5\ mm.$$

Since the array is ceiling-mounted at the height of about 3 m, the far field conditions are satisfied.

The duration of the pulsed sinusoid is chosen as T_s ms, so as to provide a reasonable range resolution [41]. Since the required range resolution of the system is roughly the area a human occupies, assuming a resolution of $\Delta R = 0.68$ m in the range to the array, The corresponding pulse width is calculated as

$$T_s = \frac{2\Delta R}{v_s} = 4\ ms$$

In order to test the narow-band assumption on the received signal, it must be shown that the following condition is satisfied

$$B\frac{D}{\lambda_1} \ll f_{c,1}$$

where B is the bandwidth of the rectangular transmitted pulse which is related to the pulse width as $B = \frac{1}{T_s}$. Therefore, since

$$B\frac{D}{\lambda_1} \approx 350\ Hz \ll 40\ kHz,$$

the narrow-band assumption is satisfied and time delays in the base-band signal can be represented as phase shift. The previously mentioned the construction of the array response vector is based on the narrow-band assumption.

In order to guarantee unambiguous range measurements inside the office space, the distance between the consecutive pulses should be more than or equal the maximum round trip time in the room area

$$T_R = \frac{2R_{max}}{v_s} = 35\ ms.$$

where T_R denotes the pulse round-trip time. Due to the reverberation of ultrasound in the indoor environment, a quiet period has to be scheduled so that echoes from the environment die before the transmission of the next pulsed sinusoid [47]. A reverberation subsidence time of RT = 25 ms was planned for the stronger echoes to die out before the next pulse interval and not to decrease the update time of the system significantly. Therefore, the pulse repetition interval of

$$T_p = T_R + \mathrm{RT} + T_s = 35 + 21 + 4 = 60\ ms$$

was chosen. Therefore, the blind speed in our system due to MTI processing is which in our system

$$v_{blind} = \frac{8.6\ mm}{2 \times 60\ ms} \approx 0.07\ ms^{-1}.$$

The range accuracy Δd of the system as mentioned earlier is chosen half of the range resolution

$$\Delta d = \frac{\Delta R}{2} = 0.343\ m$$

which corresponds roughly to the dimension of a human body in one dimensional distance-based view of the receiver array. The range accuracy corresponds to one range bin size. Since the received signal is sampled with rate $f_{s,1}$ = 200 kHz, the number of samples in one range bin, indicated as ν, is

$$\nu = \lfloor \frac{2\Delta d f_{s,1}}{v_s} \rfloor = \frac{2 \times 0.343\ m \times 200\ kHz}{343\ ms^{-}1} = 400\ samples;$$

2.4 DOA estimation

After range detection, a number of range bins are declared to contain occupants either due to the presence of a true target or due to multi-path. The data from these range bins is then processed to find the angle of arrival of the source contained. A two-dimensional conventional beam-former is then applied on the preprocessed data corresponding to each of the active range bins. For the preprocessed data, $\overline{\boldsymbol{\Delta g}}(\varrho, \varsigma)$, at the ϱth active range bin for ς th sample, the two-dimensional angular spectrum is written as

$$\Lambda(\theta, \phi) = \frac{1}{M\nu} \sum_{\varsigma=1}^{\nu} |\boldsymbol{a}(\theta, \phi)\overline{\boldsymbol{\Delta g}}(\varrho, \varsigma)|^2,$$

where Λ indicates the angular response and θ and ϕ take values from the discrete sets Θ and Φ respectively.For practical real-time implementation and the algorithm speed considerations, the azimuth and elevation angles are discretized with the accuracy of 2 degrees each.

Taking into account that in each range bin at most one occupant movement is of interest, the maximum of the angular spectrum

$$\boldsymbol{\Lambda}(\theta, \phi), \forall \theta \in \Theta \& \phi \in \Phi,$$

which corresponds to the angular location where the maximum power is received, is found. Furthermore, SNR at the detected location is computed as

$$\mathrm{SNR}(\theta_{max}, \phi_{max}, \varrho) = \frac{\max_{\theta \in \Theta, \phi \in \Phi} \Lambda(\theta, \phi)}{\epsilon(\varrho)}$$

After DOA processing, elevation, azimuth angle, corresponding range bin and which are denoted respectively as

$$\{\theta_{max}, \phi_{max}, \overline{\mathrm{SNR}}, \varrho\}$$

Where $\overline{\mathrm{SNR}}$ is chosen as the shorthand notation for $\mathrm{SNR}(\theta_{max}, \phi_{max}, \varrho)$ are stored to be supplied to the tracker for refining the location estimates by considering the temporal correlation of detections corresponding to the target.

2.5 Multi-path mitigation

After range and DOA processing, the observation points collected in one scan are then transformed to the Cartesian coordinates. Before being supplied to the tracking algorithm, data is filtered to disregard infeasible location estimates that lie beyond the physical boundaries of the environment produced due to multi-path propagation of the echoes. A scenario with a single moving occupant in the test

office is depicted in Fig 2.14(a). The red squares in the picture show the true occupant movement trajectory. The observation points formed after applying the range and DOA estimation algorithms is shown in Fig 2.14(b). As can be seen, some of the observation points lie outside the room boundary. These points are due to the multi-path propagation of the signal and are discarded by applying a simple room dimension filtering. The result after filtering is shown in Fig 2.15.

2.6 Target tracking

In order to reduce the effect of multi-path and side-lobes that a tracker is applied of the observed locations. The tracking is performed in two dimensions (x, y). A true moving target is persistent in the tracking region for several scans [73]. As a result, persistent clutter and observations formed due to side-lobes of the circular array also are classified as being a tentative target, whereas false detections caused by random noise or clutter are not correlated in time. In order to minimize misclassification between persistent false targets and the true ones, tracking and a mechanism for scoring the different tracks is implemented [62]. Tracking also is useful in addressing the problem of intermittent detections due to the MTI-processor suppressing target echoes at certain speeds [41].

For the data association and tracking algorithm described in the rest of the section, *a priori* of existence of multiple targets (whether true targets or caused by clutter or side-lobes) is assumed. The tracking algorithm is composed of four main parts; (a) observation-to-track association, (b) NCV Kalman filter-based track prediction, (c) Track scoring mechanism and (d) a list of tentative targets with their current state and tracking score. Figure 2.16 gives an overview of the tracking algorithm steps.

2.6.1 Observation-to-track data association

Observations formed in one scan are first clustered to initiate multiple tentative targets based on the proximity of the measurements. A coarse gate with size roughly equal to the area a human occupies in $x - y$ plane is used to ensure that detections due to different parts of the human target body are combined. A circular gate with radius $\sqrt{2}$ m is chosen; thus the linear resolution of a human target is 1 m in x and y directions. Measurements falling into the same proximity of one gate are clustered as one tentative target and their location is fused to produce one measured location for the corresponding target. The fusion rule for the measurements inside the same cluster at the kth scan for q_1 measurements falling in the same gate (l) is as follows

$$x_l^{(k)} = \frac{\sum_{i=1}^{q_1} x_{i,l}^{(k)} \ \overline{\mathrm{SNR}}_{i,l}^{(k)}}{\sum_{i=1}^{q_1} \overline{\mathrm{SNR}}_{i,l}^{(k)}}, \ y_l^{(k)} = \frac{\sum_{i=1}^{q_1} y_{i,l}^{(k)} \ \overline{\mathrm{SNR}}_{i,l}^{(k)}}{\sum_{i=1}^{q_1} \overline{\mathrm{SNR}}_{i,l}^{(k)}},$$

where $\overline{\text{SNR}}_{i,l}^{(k)}$ is the SNR at the location. Coordinates of the tentative targets are stored and sent to the Kalman filter to be propagated to the next scan. score calculation

2.6.2 Filtering and prediction

For track filtering, a NCV motion model [74, 75] is used to model target movement dynamics together with a two-dimensional Kalman filter. The state of the lth tentative target at scan k is presented as

$$\overline{\boldsymbol{s}}_l^{(k)} = \left[\hat{x}_l^{(k)}, \hat{y}_l^{(k)}, \dot{x}_l^{(k)}, \dot{y}_l^{(k)}\right]^T,$$

where $\hat{x}_l^{(k)}$ and $\hat{y}_l^{(k)}$ represent the estimated occupant location and $\dot{x}_l^{(k)}$ and $\dot{y}_l^{(k)}$ represent estimate of its speed. Occupant movement must satisfy the kinematic motion equation [76]

$$\boldsymbol{p}_l^{(k)} = \frac{1}{2}\ddot{\boldsymbol{p}}_l^{(k-1)}(\Delta t)^2 + \dot{\boldsymbol{p}}_l^{(k-1)}(\Delta t) + \boldsymbol{p}_l^{(k-1)}$$

where $\dot{\boldsymbol{p}}_l^{(k-1)}$ and $\ddot{\boldsymbol{p}}_l^{(k-1)}$ respectively denote the initial speed and initial acceleration of the lth target at scan k and $\boldsymbol{p}_l^{(k)} = [\hat{x}_l^{(k)}, \hat{y}_l^{(k)}]^T$ denotes position vector. Δt denotes the time between scans. Therefore, the occupant state transition at scan k is written as

$$\overline{\boldsymbol{s}}_l^{(k+1)} = \boldsymbol{A}\overline{\boldsymbol{s}}_l^{(k)} + \overline{\boldsymbol{w}}^{(k)}$$

where $\boldsymbol{A}$ is the state transition matrix expressed as

$$\boldsymbol{A} = \begin{bmatrix} 1 & 0 & \Delta t & 0 \\ 0 & 1 & 0 & \Delta t \\ 0 & 0 & 1 & 0 \\ 0 & 0 & 0 & 1 \end{bmatrix},$$

$\overline{\boldsymbol{s}}_l^{(k+1)}$ is the state of the occupant at the following scan and $\overline{\boldsymbol{w}}^{(k)}$ denotes the process noise which is the uncontrollable input (occupant acceleration) to the modeled system. The NCV model gives the expression for the state error covariance matrix as [75]

$$\boldsymbol{Q}_s = \sigma_s^2 \begin{bmatrix} \Delta t^4/4 & 0 & \Delta t^3/2 & 0 \\ 0 & \Delta t^4/4 & 0 & \Delta t^3/2 \\ \Delta t^3/2 & 0 & \Delta t^2 & 0 \\ 0 & \Delta t^3/2 & 0 & \Delta t^2 \end{bmatrix},$$

with $\sigma_s = 1$ ms^{-2} is a chosen design value.

Let $\overline{\boldsymbol{z}}_l^{(k)} = (x_l^{(k)}, y_l^{(k)})^T$ denote the combined measurement at scan k for the lth tentative target, since our system only measure target position and do not have

information about its speed; the measurement and the state of the occupant are related as

$$\bar{\boldsymbol{z}}_l^{(k)} = \boldsymbol{C}\bar{\boldsymbol{s}}_l^{(k)} + \boldsymbol{e}^{(k)},$$

where $\boldsymbol{C}$ is

$$\boldsymbol{C} = \begin{bmatrix} 1 & 0 & 0 & 0 \\ 0 & 1 & 0 & 0 \end{bmatrix}$$

and $\boldsymbol{e}^{(k)}$ is the measurement noise which is assumed to be white Gaussian with covariance matrix $\boldsymbol{Q}_e = \sigma_e^2 \boldsymbol{I}$, where $\boldsymbol{I}$ is a 2×2 identity matrix and variance $\sigma_e = 1$ m is chosen.

Upon receipt of data in a scan, the state of the target is updated using the received data within its gate and propagated ahead using the Kalman filter [66] to predict the occupant state at the following scan. The predicted location at the following scan forms the center of the corresponding target gate. In order to update the state of a (tentative) target and avoid merging of two crossing targets, the observation which is closest in distance to the predicted position of a target is chosen. Let $\bar{\boldsymbol{z}}_{i,l}^{(k)} = [x_{i,l}^{(k)}, y_{i,l}^{(k)}]^T$ denote the ith observation at the lth target gate at scan k and $\boldsymbol{p}_l^{(k)} = [\hat{x}_l^{(k)}, \hat{y}_l^{(k)}]^T$ denote the estimated target location, the chosen measurement to update the target state is

$$\bar{\boldsymbol{z}}_l^{(k)} = \min_i \|\boldsymbol{p}_l^{(k)} - \bar{\boldsymbol{z}}_{i,l}^{(k)}\|$$

Let $\hat{\boldsymbol{p}}_l^{(k|k-1)}$ denote the predicted position of the target based on measurements at the previous scan. Then each of the observations at the current scan are assumed to have a normal distribution around the predicted position

$$Pr\{\bar{\boldsymbol{z}}_{i,l}^{(k)} | \hat{\boldsymbol{p}}_l^{(k|k-1)}\} \sim \mathcal{N}(\hat{\boldsymbol{p}}_l^{(k|k-1)}, \bar{\boldsymbol{Q}}_l^{(k|k-1)})$$

where $\bar{\boldsymbol{Q}}_l^{(k|k-1)}$ denotes the related noise covariance matrix.

2.6.3 Scoring and track maintenance

In order to represent (a) the confidence in a tentative track as being a true target, (b) evaluate observation-to-track updates and (c) have a mechanism to initiate true tracks and delete false tracks or targets that have disappeared, a tracking score is used. The tracking score consists of a kinematic term and a signal-related term. The kinematic term is related to the distance of the detection from the center of the corresponding gate and the signal-related term is the SNR at the location where the detection was formed.

Let $d_{i,l}^{(k)}$ denote the distance of the ith measured location at scan k corresponding to the lth target from the predicted position $\hat{\boldsymbol{p}}_l^{(k|k-1)}$ and $\overline{\text{SNR}}_{i,l}^{(k)}$ denote the

SNR measured at that location. A score is assigned to each of the measurements within the lth target gate as

$$\Omega_{i,l}^{(k)} = \varrho_{i,l}^2 \overline{\mathrm{SNR}}_{i,l}^{(k)} e^{-d_{i,l}^{(k)}}.$$

$\varrho_{i,l}$ shows the range bin corresponding to the lth target. Since due to path loss signal power drops with the square of distance to the transmitter, square of distance is multiplied with target SNR in order to compensate for the power drop and assign a distance independent score to targets.

Therefore, the tracking score for the lth target at scan k is computed as

$$\hat{\Omega}_l^{(k)} = \min\{1, \hat{\Omega}_l^{(k-1)} + \max_i\{\Omega_{i,l}^{(k)}\}\}, \ i = 1, 2, .., q_2.$$

Where $\hat{\Omega}_l^{(k-1)}$ denotes the tracking score at the previous scan. The tracking score is upper limited to one. If in a cycle there remain unassociated measurements, they are supplied to the clustering algorithm to define new tentative targets. For the newly formed target clusters, $\hat{\Omega}_l^{(k-1)}$ is zero.

The data at scan k for each (tentative) target corresponding to the predicted state, error covariance matrix, previous locations of the target and tracking score are stored for use in the following scan.

2.6.3.1 Track maintenance (initiation, deletion, merging)

By using the track score for (tentative) targets that includes a contribution from SNR, the detection threshold can be set lower to allow for more detections (false alarm or true) [62]. The SNR-related term in the tracking score will ensure false track mitigation in the track confirmation step of the algorithm. Therefore, based on the tracking score of the targets, two thresholds are set to classify targets as tentative, confirmed or deleted. In the track maintenance process there are two main hypotheses [62]:

$\mathcal{H}_0$: Measurements assigned to a track are false alarms,

$\mathcal{H}_1$: Measurements assigned to a track are from a true target.

Based on these hypotheses, two thresholds are set for confirmation of tracks related to true targets and deletion of either false tracks or tracks related to targets that have disappeared (stopped walking or left the room). Knowing that detections from a true target must be persistent over time, a timing constraint is also introduced to lower the probability of false target acceptance. Furthermore, if in one scan no measurement is received for a target, the score of the corresponding target is decreased by a factor α and is compared to the deletion threshold for a prespecified number of scans before being disregarded. This ensures low probability of true target rejection.

$$\text{Receive no measurement at scan } k \Rightarrow \hat{\Omega}_l^{(k)} = \alpha \hat{\Omega}_l^{(k-1)}$$

where $\alpha \in [0, 1]$ is the forgetting factor.

The track maintenance logic is as follows:

$$\hat{\Omega}_l \leqslant \delta_2 \text{ for } \kappa_1 \text{ scans: Accept } \mathcal{H}_0 \text{ (delete track } l\text{)}$$
$$\hat{\Omega}_l \geqslant \delta_3 \text{ for } \kappa_2 \text{ scans: Accept } \mathcal{H}_1 \text{ (confirm track } l\text{)}$$
$$\delta_2 < \hat{\Omega}_l < \delta_3 : \text{continue test (tentative target)}$$

Here δ_2 and δ_3 are respectively track deletion and track confirmation thresholds, and κ_1 and κ_2 are the number of test scans for deletion and confirmation of the track respectively. δ_2 is set equal to the detection threshold δ_1 so that a true target rejection probability does not exceed the probability of missed detection. δ_3 is set above δ_1 so that tracks caused by clutter and side lobes that are persistent in time but have a smaller tracking score than true targets would be tracked, but not confirmed as true targets, at this step of the algorithm. κ_1 and κ_2 are set based on the latency requirements of the system. The scoring mechanism is summarised in Fig 2.17 [62]. The solid line shows the evolution of tracking score of a single target as more time scan data become available.

Furthermore, a track merging logic is applied for the situations when two closely-spaced tracks are formed due to initiation of tracks from different parts of the same human target body. In order to assure that the merger does not merge crossing targets, a logic based on the closeness of state vector of different (tentative) targets is used as follows

$$\|\overline{\boldsymbol{s}}_j - \overline{\boldsymbol{s}}_i\| < C_{th} \text{ for } \kappa_3 \text{ scans} \Rightarrow \text{drop the redundant track}$$

where $\overline{\boldsymbol{s}}_j$ and $\overline{\boldsymbol{s}}_i$ are the state estimates of the jth and ith track respectively and the redundant track refers to the track that has existed for a shorter time.

Finally, the result of the single occupant movement after applying the tracker is shown in Fig 2.18.

2.7 Conclusions

In this chapter, we proposed a real-time ultrasonic granular indoor presence sensing system based on a circular receiver array. At the first stage, the received pulse echoes are possessed and the range of the occupant is obtained. At the second stage, The DOA of the potential occupant in the active ranges is estimated using the conventional beam-former. The 2D location of the target is computed using the estimated range and DOA. Because of multi-path that causes false alarms and missed detections, a tracking algorithm based on NCV Kalman filter and a tracking score mechanism to distinguish between true and false tracks is proposed. The experimental results of a single-target scenario are presented.

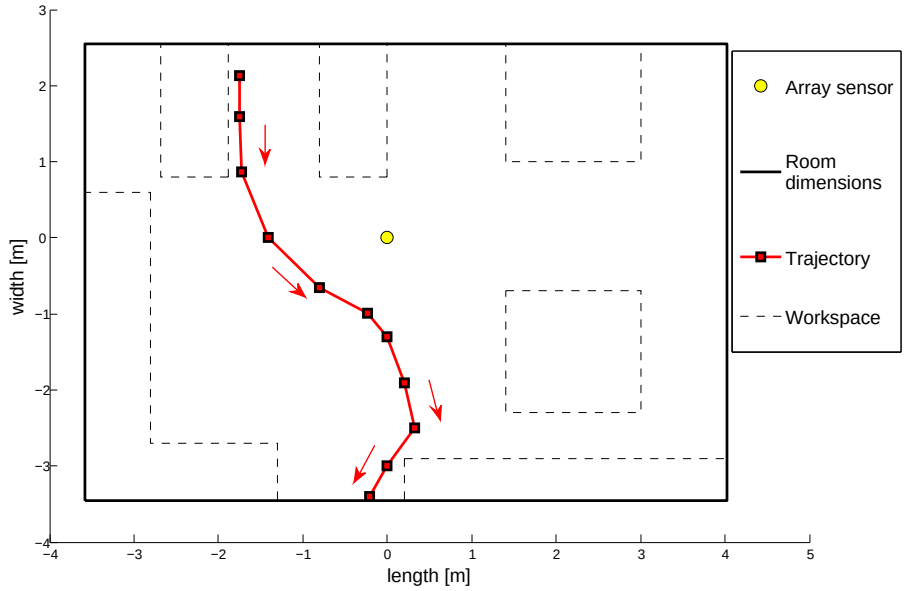

(a)

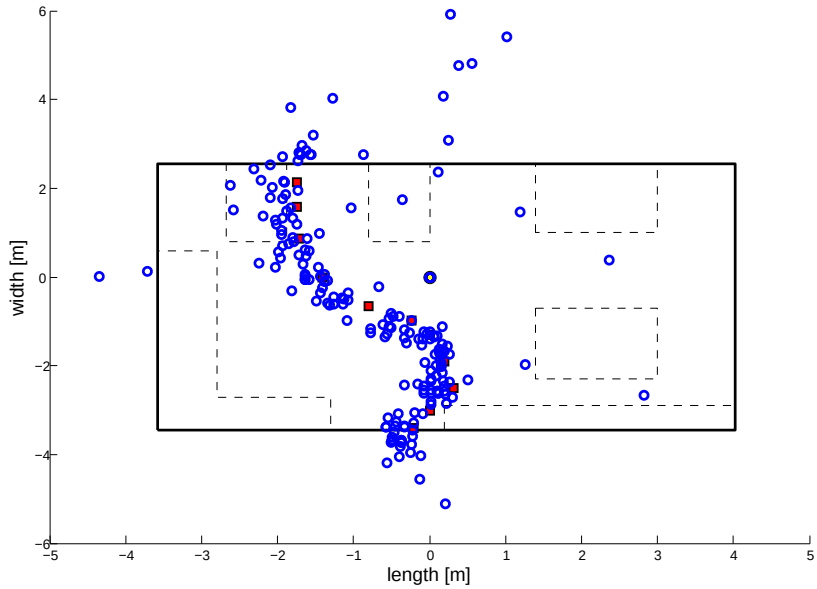

(b)

Figure 2.14: (a) A single-ocupant movement scenario inside the test room, (b) Observation points formed after range and DOA estimation

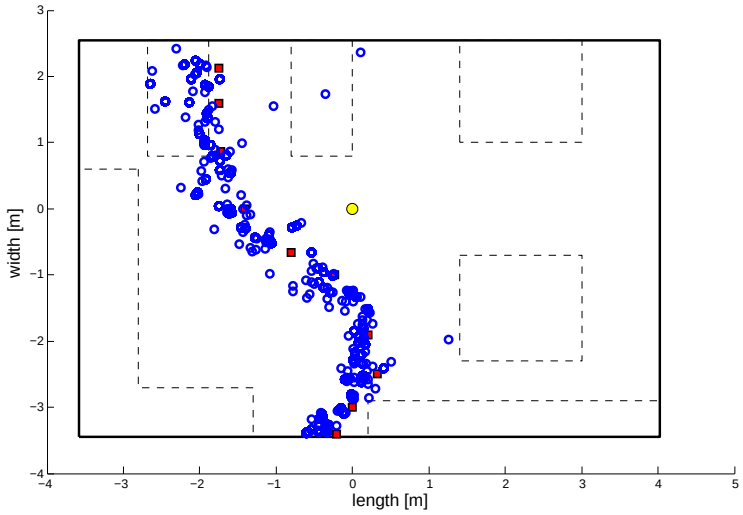

Figure 2.15: Observation points for a single moving occupant after filtering based on the room dimensions.

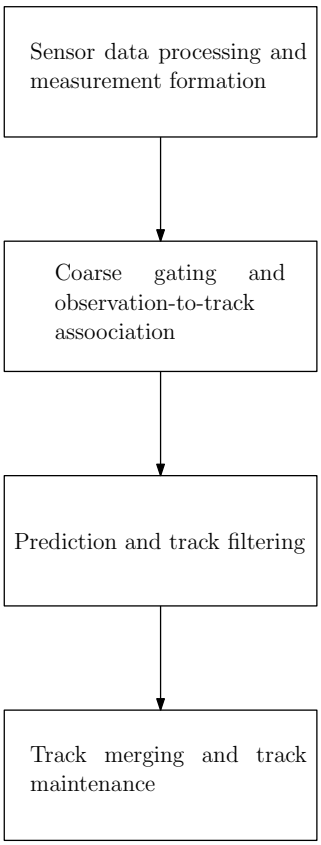

Figure 2.16: Tracking algorithm procedure.

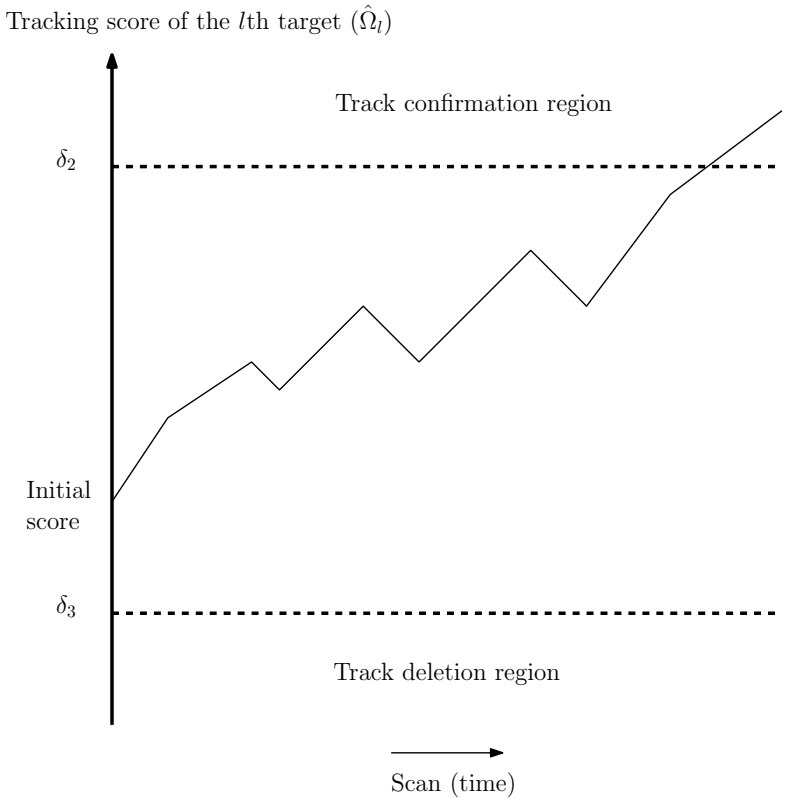

Figure 2.17: Track scoring mechanism.

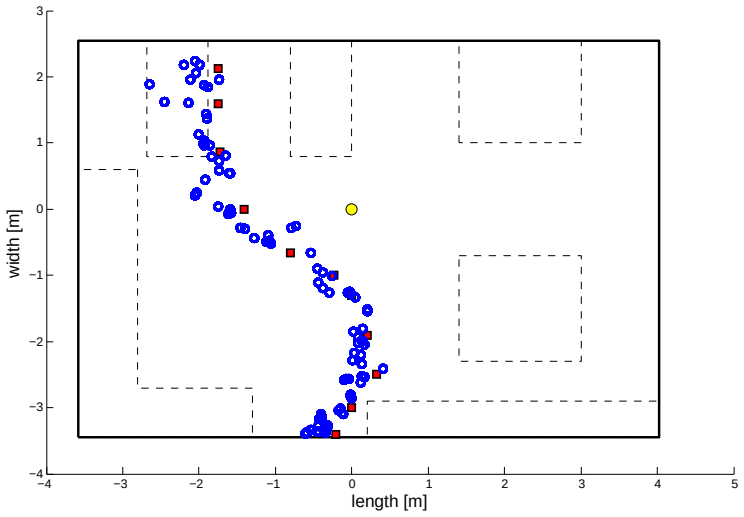

Figure 2.18: Presence sensing result after applying the tracker.

Combined Control Messaging and Positioning

3

In this chapter, we detail the design of the communication system that exploits the existing wide-band circular array receiver (as explained in Chapter 2) and one or more mobile transmitters. The transmitter which is the speaker of the consumer laptop or smart-phones, facilitates the room occupants with the ability to send control commands for adjusting the room attributes according to their needs. The receiver further applies beam-forming on the received message to estimate the DOA of the transmitted signal to provide the controller with the specific zone in which the occupant is located for the changes to be applied in the corresponding region. To establish the communication, at the occupant side, there is a mobile device capable of producing near-ultrasonic transmissions. For instance, a commercial audio speaker of a laptop or smart-phone may be used; Most speakers are capable of producing near-ultrasonic frequencies in the range of 18-22 kHz [52]. We use 5 bits to encode user requests (e.g. increase or decrease illumination level by specific amount, light color level etc.), after applying error correcting codes, on-off keying (OOK) communication scheme at the carrier frequency of 20 KHz is used to transmit the encoded command. Line-of-sight is assumed during user signalling, as is common in remote control actions. At the circular array receiver, upon detection of the presence of signal, the communication signal is band-passed. The signal is then decoded and DoA processing is performed to determine the region from which the message was transmitted. This information is then sent to the lighting controller where the requested user changes are executed within the specified workspace region.

3.1 System description

The near-ultrasonic communication system is composed of two major parts; (i) Circular array receiver (ii) Speakers of one or more mobile devices (laptop or smart-phone). The speaker of each mobile device is set to operate at the near-ultrasonic central frequency of $f_{c,2}$. The circular array receiver is the same as the one explained in Chapter 2. Due to the wide-band characteristics of the receiver (see Appendix 1), it is possible to incorporate the presence sensing system (at the center frequency of $f_{c,1} = 40$ kHz) and the communication system (at the center frequency of $f_{c,2} = 20$ kHz) in one receiver. Further, band-pass filtering is applied to eliminate the potential interference between the two systems and to eliminate unwanted frequencies.

3.1.1 Receiver beam pattern

The circular array receiver is the same as the one described in Chapter 2. In the communication system, mobile transmitters are set to work at the carrier frequency of $f_{c,2} = 20$ kHz which is lower than $f_{c,1} = 40$ kHz used for presence sensing. The beam-pattern of the array at frequency $f_{c,2}$ is depicted in Fig 3.1(a). In this scenario, since

$$\Delta m < \frac{\lambda_2}{2} = \frac{v_s}{2f_{c,2}} = 8.6\ mm,$$

no side-lobes appear in the spatial response (Fig 3.1(b)); However, the beam-width increases and the angle estimation accuracy decreases.

3.1.2 Room configuration and workspace regions

As explained in Chapter 2, The circular array receiver is installed in approximately the center of the ceiling of an office room of height $\hat{h}$, width $\hat{w}$ and length $\hat{l}$ as depicted in Fig 3.2. Moreover, there exist 12 luminares located evenly at the ceiling of the test office. There are 4 work-spaces in the room are shown in red in Fig 3.2.

3.2 Communication system

In this section, the design of the communication system for lighting remote control application is explained. The system consists of one or more mobile transmitters and the circular array receiver. Due to the ultrasonic channel properties and absence of a direct physical link between the transmitter and receiver, at the transmitter side asynchronous communication with OOK modulation was chosen. On the other hand, at the receiver side a frame synchronization technique based on high-correlation sequences and energy detection is applied to decode the lighting control command. Moreover, to increase the robustness of the system, BCH codes are used. In addition, assuming the alignment of the mobile transmitter is such that there is a direct path between the transmitter and the receiver, DOA of the received signal is used to locate the region in which the control command should be executed.

3.2.1 Transmitter

In order to transmit lighting control commands, as illustrated in Fig 3.3, the command is first translated into a binary sequence $\{b_1[n]\}$ of length L_1. After adding error correcting codes to the sequence, the resulting encoded sequence $\{b_2[n]\}$ of length L_2 is en-framed to a sequence $\{b_3[n]\}$ of length L_3. One instance of the framed bit sequence is shown in Fig 3.4(a). The framing is done in order

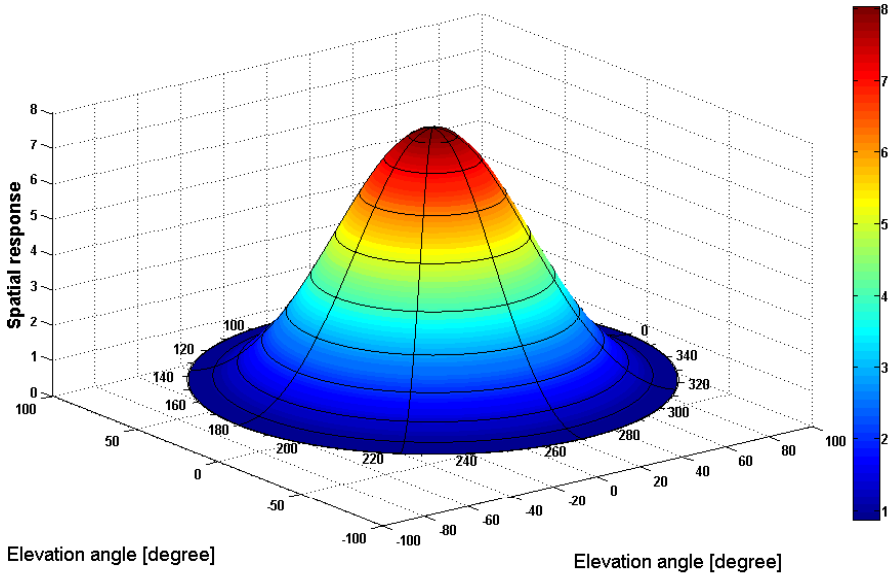

(a)

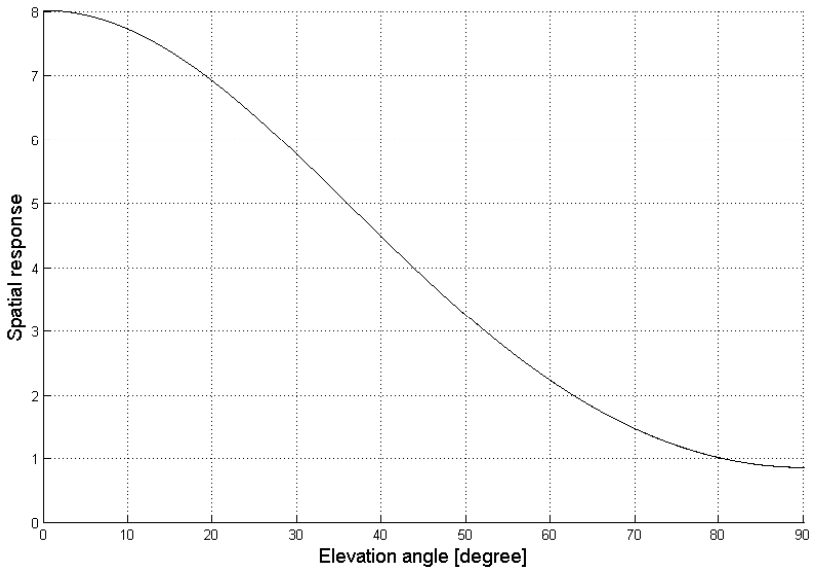

(b)

Figure 3.1: (a) Spatial response of the UCA at 20 kHz,(b) Spatial response of the UCA at 20 kHz versus elevation angle.

to establish an asynchronous communication between the mobile device and the receiver array. The data frame consists of a preamble part (consisting of three marker sequences $\{g_M[n]\}$, each of length L_2 and a training sequence $\{g_T[n]\}$ of length L_2) continued by the payload as shown in Fig 3.5.The resulting binary

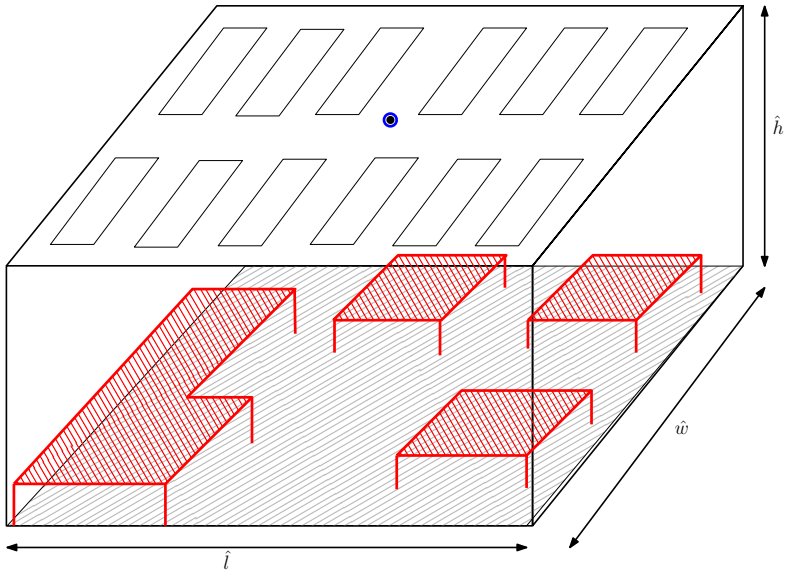

Figure 3.2: Room configuration and work-spaces.

sequence $\{b3[n]\}$ after framing is then assigned unipolar voltage levels $a_n \in \{0, A_c\}$ ($a_n = A_c$ V when a binary 1 is sent and $a_n = 0$ V when a binary 0 is sent). The coded digital signal is represented in analog form by a sequence of Dirac pulses as

$$d_c(t) = \sum_{n=1}^{L_3} a_n \delta(t - nT_b)$$

where $d_c(t)$ denotes the coded analog signal, δ is the Dirac delta function and T_b represents the bit duration. The coded signal is then up-sampled to the speaker sampling frequency of $f_{s,2}$. Number of samples in one bit interval $n_{s,1}$ is stated as

$$n_{s,1} = \lfloor f_{s,2} T_b \rfloor.$$

After up-sampling, square-root raised cosine pulse shape [77] $h_{src}(t)$ is assigned to the unipolar base-band data signal to generate the base-band signal $q_t(t)$

$$h_{src}(t) = \frac{4\alpha_r}{\pi\sqrt{T_c}} \frac{\cos(\frac{(1+\alpha_r)\pi t}{T_c}) + \frac{T_c \sin(\frac{(1-\alpha_r)\pi t}{T_c})}{4\alpha_r t}}{1 - (\frac{4\alpha_r t}{T_c})^2}$$

where α_r is the roll-off factor and T_c indicates the truncation length of the filter in symbol periods. We use a pair of square-root raised cosine filters at the transmitter

and receiver so as to get a raised cosine filter at the output of the receiver matched filter to satisfy the Nyquist criterion and avoid inter-symbol interference(ISI) by providing zero crossing at adjacent symbol picks. The signal obtained after applying the pulse shaping filter on the framed data is depicted in Fig 3.4(b) for one data frame. The base-band signal is then multiplied with the carrier frequency at $f_{c,2}$ and transmitted through the mobile device speaker. The transmitted OOK signal is represented by [78]

$$s_2(t) = A_c q_t(t) cos(2\pi f_{c,2} t),$$

where $s_2(t)$ is the transmitted signal. $s_2(t)$ for one data frame is illustrated in Fig 3.4(c).

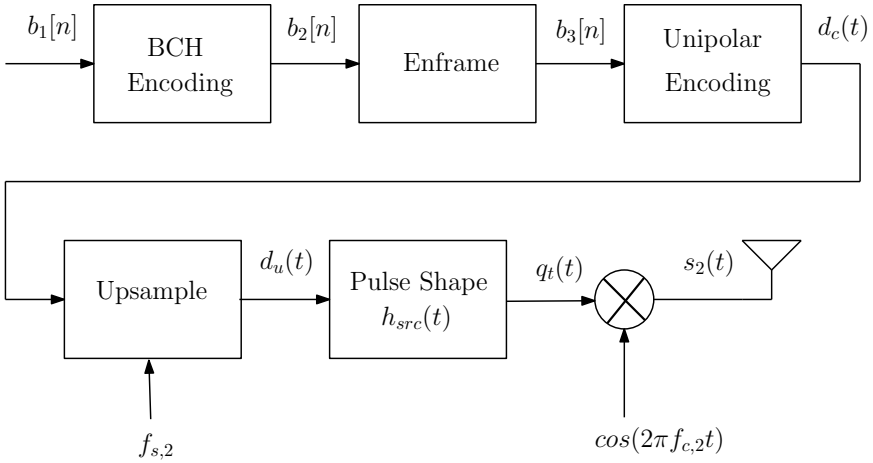

Figure 3.3: Transmitter block diagram.

3.2.2 Indoor ultrasound channel

Indoor ultrasonic channel is a time varying multi-path fading channel. As explained in Chapter 2, equation 2.3, the multi-path channel can be modeled as [79]

$$h_c(t) = \sum_{n=1}^{N(t)} \beta_n(t) e^{-j2\pi f_{c,2} \tau_n(t)} \delta(t - \tau_n(t))$$

where $h_c(t)$ denotes the base-band channel impulse response. Therefore, the received low-pass signal $q_2(t)$ can be considered as the convolution of the transmitted base-band pulse with the ultrasonic channel.

$$q_r(t) = q_t(t) * h_c(t) + \chi(t)$$

where χ indicates the base-band additive white Gaussian noise.

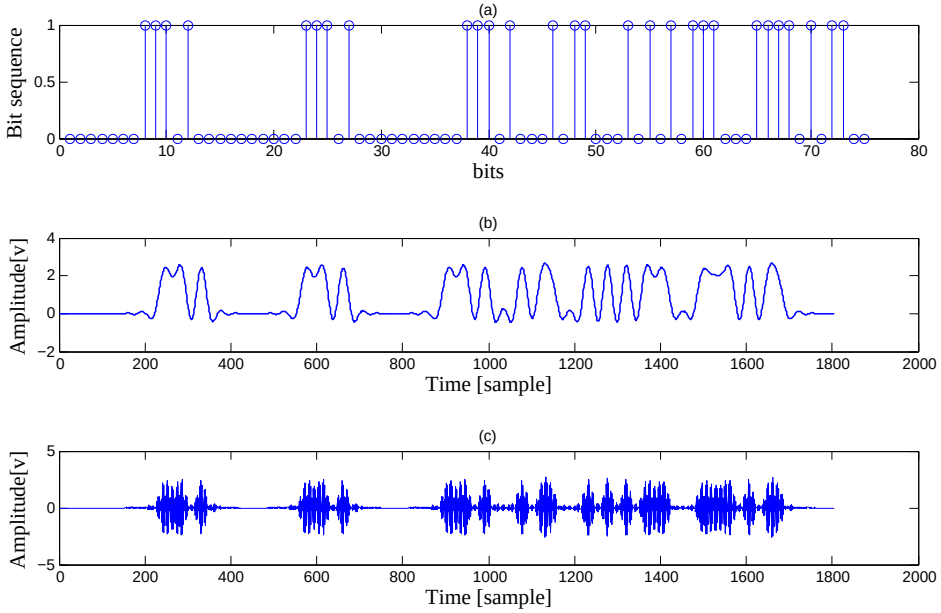

Figure 3.4: Transmitter steps.

Marker	Marker	Marker	Traning	Payload

Figure 3.5: Data frame structure.

As mentioned earlier in Chapter 2, ultrasound experiences reverberation when propagating in an indoor environment. Therefore, longer multi-path components reach the receiver. However, the amplitude of the components degrade with time due to pass-loss. Since the purpose of this research was to find a practical air-borne ultrasonic communication system for remote control design applications that provides the possibility for the receiver to location of the transmitter, it is assumed that the orientation of the mobile device is such that a clear line-of-sight (LOS) exists between the transmitter and the array receiver. The channel was empirically studied. A typical LOS channel impulse response in the test office is shown in Fig 3.6.

Which shows the LOS component is received with significantly higher amplitude than other multi-path components. The demodulator in the receiver is therefore synchronized to this component As a result, if we set the detection threshold above the multi-path component level then there is only one dominant ray and no resolvable multi-path, and the channel can be assumed as flat-fading. This assumption only implies if the LOS is attained between the mobile device and the

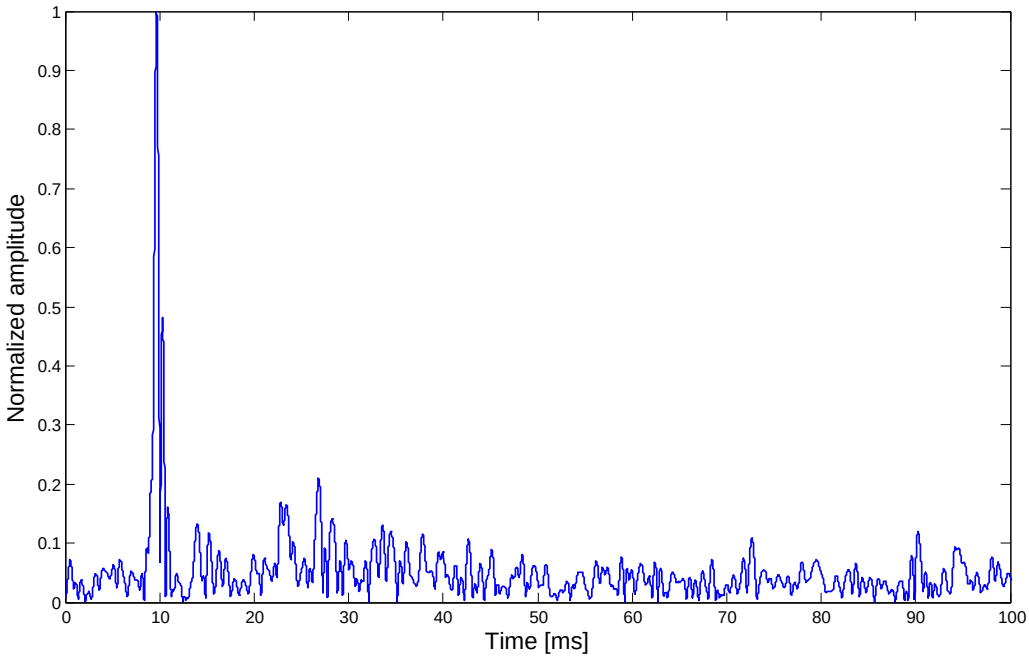

Figure 3.6: Typical LOS channel in the test room.

receiver.

Apart from noise and multi-path propagation, due to the slow propagation speed of the ultrasound as compared to light and other radio frequencies, a small movement causes a significant Doppler shift.

Moreover, It is shown in [52, 14] that sound at higher frequencies in the range of ultrasound is very directional. This means that the intensity of ultrasound is much higher in front of the speaker and as a result, the maximum range that it can travel is larger. Thus, The orientation of the mobile device with respect to the receiver array has a significantly influences the reception quality. In addition, high frequency sound is easily blocked by the objects along the path [52]. Therefore, we assume LOS alignment of the mobile device speaker and the receiver and that no objects obscure this direct LOS.

3.2.3 Receiver

The receiver of the communication system as shown in 3.7 consists of two major parts. The first part which is constantly running at the receiver signal processing unit is used to detect the presence of signal in the operating band of the communication system. The second part, acquires a block of the received data samples,

which are provided by the signal detection part, and after achieving synchronization decodes the control command and estimates the DOA of the signal through beam-forming.

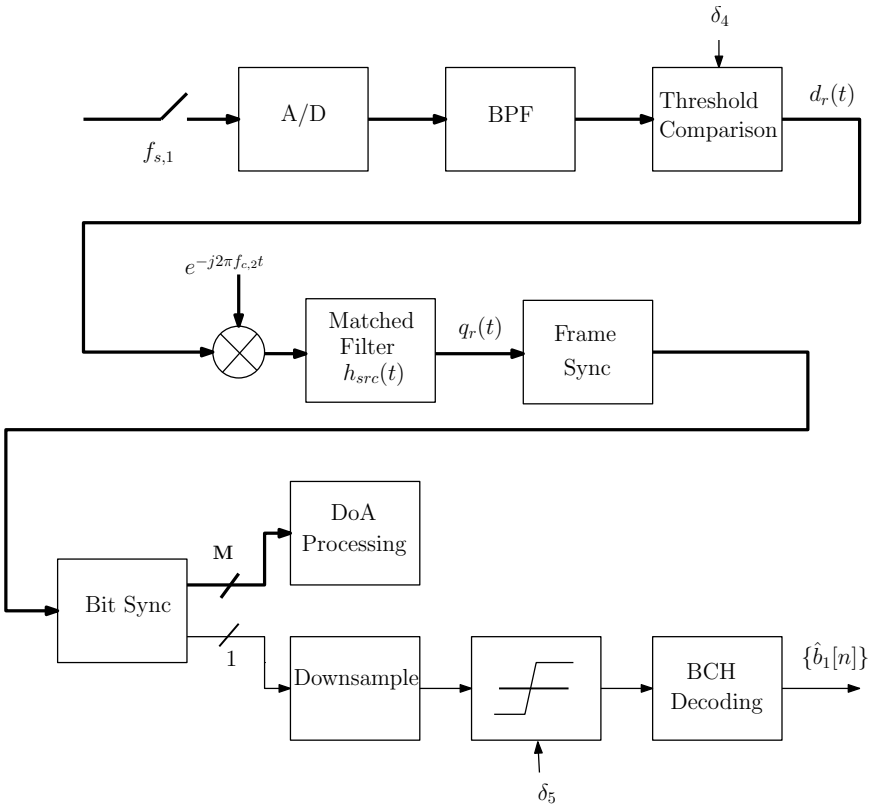

Figure 3.7: Receiver block diagram.

3.2.3.1 Signal detection

The analog signal received by M antenna elements is first sampled at the receiver sampling frequency $f_{s,1}$ and quantized. In order to detect the presence of signal at the communication system operating frequency $f_{c,2}$, the receiver constantly performs bandpass filtering on a time window of the received samples, integrates the received power over that time window and compares it with the detection threshold δ_4 that is set above the bandpass noise power ($P_{FA} = 10^{-6}$). The bandpass filter is centered around $f_{c,2}$ with the bandwidth of B_2. Upon detection of the signal, a portion of the buffered and upcoming samples $d_r(t)$ which roughly correspond to the size of a data packet are chosen for further processing.

3.2.3.2 Decoding and DOA processing

Conversion to base-band The receiver implements a non-coherent detection [80] followed by DoA processing and decoding as illustrated in Fig 3.7. The received data block through the M receiver channels, sampled at the receiver sampling frequency $f_{s,1}$ is first complex conjugate demodulated with the zero-phase reference signal $e^{-j2\pi f_{c,2}t}$ and matched filtered with the square-root raised cosine $h_{src}(t)$ pulse shape that is the same as the transmitter pulse shaping filter. Therefore the overall pulse shape of the system is a raised cosine pulse shape. After matched filtering, base-band signal $q_r(t)$ is attained. Let the mth sample of the base-band signal be denoted as $q_r[m] = q_r[m/f_{s,1}]$, it is computed as

$$q_r[m] = \sum_{n=-T_c n_{s,2}}^{T_c n_{s,2}} d_r[n] h_{src}[m-n]$$

where $d_r[n]$ is the mth sample of the received data packet and $n_{s,2}$ is the number of samples contained in one bit duration as

$$n_{s,2} = \lfloor f_{s,1} T_b \rfloor.$$

An instance of the raw received data, down-mixed and matched filtered is shown in Fig 3.8(a),(b) and (c) respectively.

Frame synchronization After conversion to base-band, In order to determine whether the data block actually contains a data frame or is merely a false alarm and to perform frame and coarse bit synchronization for down-sampling and decoding purposes, the structure in the preamble of the packet is exploited. As explained earlier, the preamble consists of three identical high-auto-correlation sequences $\{g_M[n]\}$ (named as marker) and a training sequence as shown in Fig 3.5. First, cross-correlation of the bandpass received data samples with the known marker sequence up-sampled to the receiver sampling frequency is computed as

$$y_r[m] = \sum_{n=1}^{4L_2 n_{s,2}} q_r[n] \hat{g}_M[n+m]$$

where $y_r[m]$ is the correlation output and $\hat{g}_M[m]$ denotes the up-sampled marker sequence to the receiver sampling frequency. After computing the correlation output, three consecutive correlation peaks with distance equal to $L_2 n_{s,2}$ are found and compared against a threshold to find the beginning of the training sequence and maintain a coarse timing synchronization [81, 82]. Marker sequences for synchronization purposes need to have a high auto-correlation and low cross-correlation with other sequences [83]. Three consecutive peaks are considered due to the

small size of the marker sequence used in the data packet which limits its auto-correlation and cross-correlation performance. Moreover, due to the presence of noise and other channel anomalies, received voltage level experiences random variations which further reduce the auto-correlation and cross-correlation performance. After finding the first correlation peak that exceeds a predetermined threshold, we look for the second peak in the vicinity of $n_{s,2} \times L_2$ samples apart from the first one that exceeds the threshold. The third peak is found in a similar manner. After the detection of the third peak, the start of the training sequence is found in the next $n_{s,2} \times L_2$ samples from the third peak. This gives a coarse synchronization to the start of the first bit of the training sequence. In the next step, the synchronization is refined. An instance of the correlation output is shown in Fig 3.8. The red arrows correspond to the detected consecutive peaks.

Bit synchronization The cross-correlation synchronization finds the coarse bit time of the first bit in the training sequence. Since the training sequence is known, a search for the peak of the bit during the first bit interval is performed to maintain fine timing synchronization.

Decoding and DOA estimation After maintaining the bit synchronization, a short block of the following samples of the data block corresponding to one bit duration is supplied to the DoA estimation algorithm explained in Chapter 2, Section 2.4 to determined the angles from which the control command is received. Furthermore, the data block is down-sampled to bit rate. To set an adaptive threshold for making the decision on the received down-sampled voltage level corresponding to '0' or '1' bit, the average voltage level of the '0' bits as well as '1' bits in the training sequence are computed and the threshold δ_5 is set in the middle of the two levels to ensure minimum bit error probability and equal bit error probability for '0' and '1'. Thereafter, BCH decoding is performed on the resulting binary sequence to reduce the random bit errors. An example of the transmitted encoded binary command and the corresponding received voltage levels is shown in Fig 3.9. The red line corresponds to the adaptive threshold set for this received data.

3.3 Practical design considerations

In this section, the design parameter choices for the communication system are provided.

3.3.1 Transmitter design parameters

Standard laptop and smart-phone speakers sample the audio streams at the sample rate of $f_{s,2}$=44.1 kHz. Laptop and mobile phone speakers hardware are optimized for working at audible frequencies (below 20 kHz) but are shown to be capable

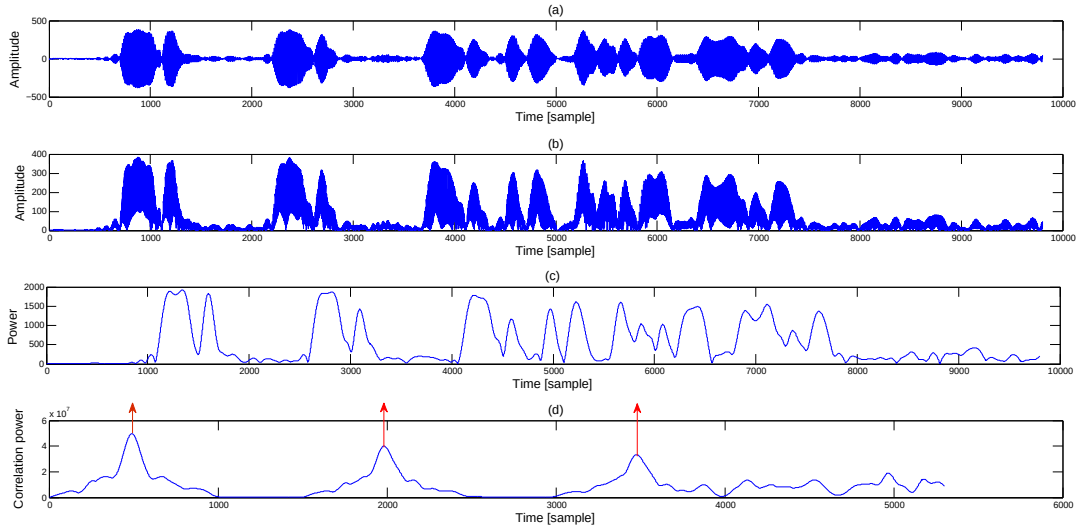

Figure 3.8: Communication system transmitter block diagram.

of producing inaudible frequencies up to 22 kHz [13, 14, 15]. For the design of the communication system, available frequency was assumed in the near-ultrasonic band of 18-22 kHz. Although the upper limit of the human hearing range is 20 kHz, at frequencies higher than 18 kHz most adults have significantly decreased hearing ability. The carrier frequency was chosen in the center of the available frequency interval at $f_{c,2}$=20 kHz. The uniform circular array receiver has a wide-band sensitivity pattern that covers the aforementioned frequency range.

In order to choose the base-band pulse duration, taking into account the available bandwidth, real-time implementation requirements and assuming the LOS channel model as discussed in Section 3.3, a bit rate of $r_b = 2$ kbps which corresponds to the bit duration of T_b=500 μs was chosen. Therefore, the number of samples contained in one bit duration after up-sampling to the receiver sampling frequency is

$$n_{s,2} = \lfloor f_{s,1} T_b \rfloor = \lfloor 44.1\ kHz \times 500\ \mu s \rfloor = 22\ samples.$$

Moreover, binary constellation is used in order for the system to have high robustness against noise.

In order to avoid ISI, the bit duration must be chosen larger than the reverberation time of the ultrasound signal which is about 60 ms in the room under consideration. This gives rise to a pulse duration of about 17 ms which is inappropriate for the real-time applications. Therefore, by assuming LOS orientation of the mobile device with the receiver array, as discussed earlier since only one significant path exists, we reduce the bit duration. This assumption gives rise to

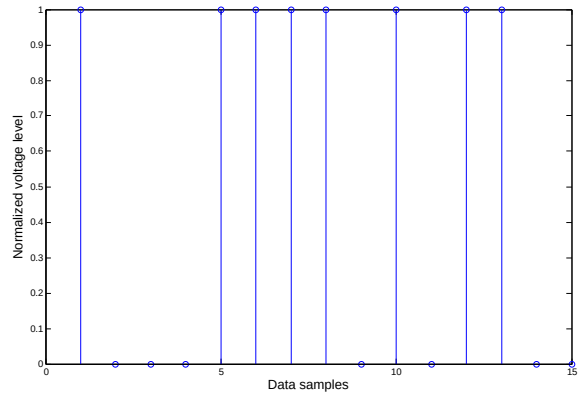

(a)

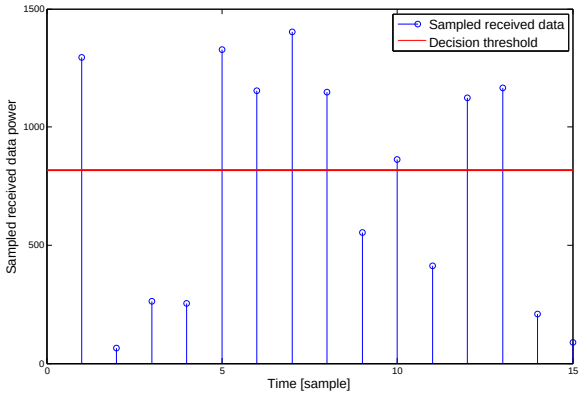

(b)

Figure 3.9: (a) Original encoded payload,(b) down-sampled received data and the adaptive threshold.

performance degradation if the LOS assumption is violated.

In the communication system operating frequency, the wavelength λ_2 is equal to

$$\lambda_2 = \frac{v_s}{f_{c,2}} = \frac{343}{20\ kHz} = 17.2\ mm.$$

Therefore, due to ceiling mounted configuration of the array, again the far field assumption holds. More specifically, the three conditions

$$R \gg D \approx 12\ mm,\ R \gg \lambda_2 \approx 17.2\ mm,\ R \gg \frac{2D^2}{\lambda_2} \approx 169\ mm$$

are satisfied. Where R is the distance of the mobile device relative to the array receiver and D is the dimension of the array. [64].

In order to localize the pulse both in frequency and time domain, perform pulse amplitude tapering to reduce the buzzing sound caused when operating at maxi-

mum speaker gain and have a robust pulse shape against ISI, we use a square-root raised cosine pulse shape. The square-root raised cosine filter for pulse shaping is used as a pair in the transmitter and the receiver so that the matched filtered received signal would have a raised cosine pulse shape. Ideal square-root raised cosine pulse shapes have infinite time duration. Therefore, they need to be truncated to a finite length. The chosen truncation length for the system is $T_c = 10$ symbols and the roll-off factor is set to $\alpha_r = 0.3$. Therefore, the transmitted pulse bandwidth B_1 would be

$$B_1 = \frac{1}{2}(1 + \alpha_r)r_b = 1.3\ kHz$$

which indicates that the occupied pass-band frequency range is in the range [18.7,21.3] kHz which fits within the available bandwidth.

We assume that the user-driven command for the control of lighting is translated into a binary sequence of length $L_1 = 5$ bits.Therefore, 32 different commands can be accommodate. These commands can include light intensity by specific level, light color and mood or other light related features. The binary command is then encoded to a sequence of length $L_2 = 15$ bits using a BCH code of (5,15,7) that due to the hamming distance of 7 can correct up to 3 random errors.

For the frame synchronization, the chosen marker sequence $\{g_M[n]\}$ in the transmitted data frame, is a Gold code [83] of length $L_2 = 15$ bits. Gold code is chosen due to its high auto-correlation and low cross-correlation with other bit sequences. How ever, due to the limited size of the marker sequence, the cross and auto-correlation performance is reduced. Therefore, for robust synchronization three repetition of the same code is used. The choice of the number of required marker sequences was verified empirically. Moreover, the chosen training sequence $\{g_T[n]\}$ of length $L_2 = 15$ bits includes approximately the same number of zeros and ones, starting with a one to perform fine bit synchronization. Therefore, the number of bits in one data packet is

$$L_3 = 5 \times L_2 = 75\ bits.$$

3.3.2 Receiver design parameters

Due to the complexity advantage of non-coherent receivers and difficulty of estimating the carrier phase without a physical link between the transmitter and the receiver array, non-coherent detection was chosen. Typical modulation techniques used for non-coherent detection are OOK, pulse-position modulation (PPM) and frequency-shift keying (FSK)[84]. FSK is not appropriate for our channel-receiver combination due to different effect of the multi-path fading channel on different frequency bands and limited available bandwidth. Among OOK and PPM, OOK with adaptive decision threshold was chosen.

The receiver sampling frequency as previously mentioned is equal to $f_{s,1} = 200$ kHz. Therefore the number of samples in one bit duration is

$$n_{s,2} = \lfloor f_{s,1} T_b \rfloor = \lfloor 200\ kHz \times 500\ \mu s \rfloor = 100\ samples.$$

The array receiver is wide-band, covering the frequency range of 100 Hz to 80 kHz. Therefore, presence sensing system and the communication system can be accommodated in the same receiver by applying suitable bandpass filtering to eliminate the potential interference between the two frequency bands and to remove the unwanted frequencies. Due to the possible movement of the mobile device, assuming the maximum speed of the movement of the mobile device to be $v_{max} = 4\ ms^{-1}$, the corresponding maximum Doppler frequency shift is

$$f_{D,max} = \pm \frac{f_{c,2} v_{max}}{v_s} = \frac{20kHz \times 4ms^{-1}}{334} \approx \pm 240\ Hz.$$

At the receiver side, the bandpass filter is centered around the carrier frequency $f_{c,2}$ with the bandwidth that can incorporate the complete base-band pulse, possibly frequency shifted due to Doppler effect when there is movement. Therefore, the bandwidth of the receiver bandpass filter is set to

$$B_2 = \frac{1}{2}(1 + \alpha_r) r_b + f_{D,max} \approx 1.6\ kHz$$

were B_2 denotes the bandwidth of the receiver bandpass filter.

3.4 Conclusions

In this chapter, the proposed combined ultrasonic communication system and positioning algorithm was presented. The transmitter and receiver design was explained. The transmitter runs on a laptop or smart-phone and using the built-in speaker, OOK-modulated, framed control command is sent through the ultrasonic channel in the indoor environment. The signal is received by the circular array receiver. Decoding and DOA estimation is performed at the receiver side to extract the control command and the occupant zone to apply the required changes in the corresponding workspace region.

Experimental and Simulation Results

4

In this chapter, the performance of the proposed indoor granular presence sensing algorithm described in Chapter 2 is evaluated empirically. The experiments are conducted in real-time under predefined test conditions when two or three occupants are present in the office room under test. Furthermore, in the rest of the chapter, the efficacy of the proposed communication system explained in Chapter 3 is assessed both empirically and based on simulations.

4.1 Experimental results of the granular presence sensing system

In this section, we present the results of the real-time experiments conducted in the office room under test for the case where two or three occupants were present. The single-occupant experimental results were already discussed in Chapter 2.

4.1.1 Experiment settings and design parameters

The experiments were performed in an office room with length $\hat{l}$ =7.6 m ,width $\hat{w}$ =6 m and $\hat{h}$ =3 m as partially depicted in Fig 4.1. The trajectories of the movements of the occupants were marked on the floor prior to the start of the experiment as illustrated in Fig 4.1. An 8-element uniform circular array prototype with a co-located single transmitter shown in Fig. 4.2, was installed in a ceiling-mounted configuration in the office room as displayed in Fig 4.3. The origin was located at the sensor at roughly the center of the ceiling (see Fig. 4.4(a) for location), i.e. $x = 0; y = 0; z = 0$. The room parameters are summarized in Table 4.1. The transmitter was of model 400EP14D [1] at the central frequency $f_{c,1} = 40$ kHz, bandwidth 2 kHz and with a broad-beam profile. A driving voltage of 9 Vpp was chosen for the transmitter to cover the complete room area without causing excess implications. The receiver array consisted of eight elements of model SPM0204HD5 [2] with an inter-element separation of 4.6 mm (see Appendix 1 for further information about the transmitter and the receiver model).

The parameters of the transmitted waveform were $T_s = 4$ ms and $T_p = 60$ ms. Since the receiver uses two consecutive pulses for MTI processing, the time between scans is 120 ms. This lower limits the update time of the system for producing the location estimates of the occupants. Parameter $\kappa_2 = 10$ was chosen which gives a latency of at least 1.2 s before the tracker confirms a true target. Furthermore,

$\kappa_1 = 20$ was chosen which indicates the tracker waits at least 2.4 seconds before a disappeared target is deleted. For real-time implementation, a granularity of 2 degrees was chosen for DOA estimation in both azimuth and elevation angles. The detection threshold δ_1 was chosen as discussed in Chapter 2, Fig 2.11. Track score evaluation threshold δ_2 is set equal to the detection threshold δ_1 so that a true target rejection probability does not exceed the probability of missed detection. δ_3 is set 10 times δ_1 so at least 10 consecutive detections of a target is needed to confirm the target as being a true target. The design parameters of the transmitter, receiver and tracker are summarized in Table 4.2, Table 4.3 and Table 4.4 respectively.

Furthermore, the received signals from the circular array are first sampled and digitized through analog-to-digital converters and are fed to a desktop computer for further signal processing in MATLAB.

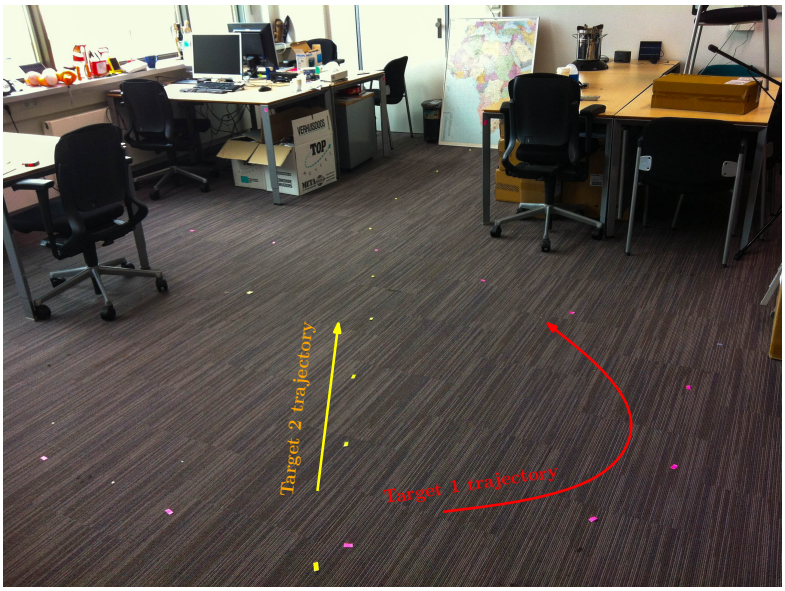

Figure 4.1: Workspace position and occupant trajectory inside the test office.

$\hat{l}$	7.6 m
$\hat{w}$	6 m
$\hat{h}$	3 m
R_{max}	6 m

Table 4.1: Room parameters.

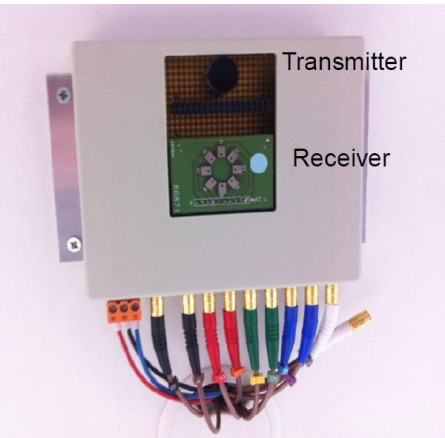

Figure 4.2: Sensor prototype at ceiling.

Figure 4.3: Array sensor position in the test office.

4.1.2 Experimental results

We consider the granular detection and tracking performance analysis for two multiple-occupant scenarios in an office environment as depicted in Fig. 4.4(a) and 4.5(a). The solid lines at the edges denote the physical boundaries, while

Model	400EP14D
$f_{c,1}$	40 kHz
Driving voltage	9 Vpp
T_s	4 ms
T_p	60 ms
λ_1	8.6 mm

Table 4.2: Transmitter design parameters.

Model	SPM0204HD5
Array geometry	circular
r	6 mm
Δm	4.614 mm
$f_{s,1}$	200 kHz
Δd	0.343 m
P_{FA}	10^{-3}

Table 4.3: Receiver design parameters.

α	0.8
κ_1	20 scans
κ_2	10 scans
κ_3	4 scans
δ_2	δ_1
δ_3	$10\times$ δ_1
C_{th}	0.1

Table 4.4: Tracker design parameters.

the dashed lines indicate workspace regions with furniture. For the first scenario, the first occupant moves along the track marked by the red squares while the second occupant follows the track marked by green triangles. Both occupants start simultaneously from the points A and B as depicted in Fig. 4.4(a). The occupant marked by green triangles first passes the intersection as the occupant market by red squares follows. This is to guarantee that one occupant does not obstruct the view of the receiver array from the second occupant. The results of the estimated trajectory upon detection and tracking are shown in real-time as black circles and blue diamond for the first and second occupant respectively in Fig. 4.4(b).

In the second scenario, three occupants are present in the room as shown in Fig. 4.5(a). The first occupant Indicated by the cyan star has small movements while seated on a chair at the specified location. The two other occupants move along the tracks designated by the red squares and green triangles respectively.

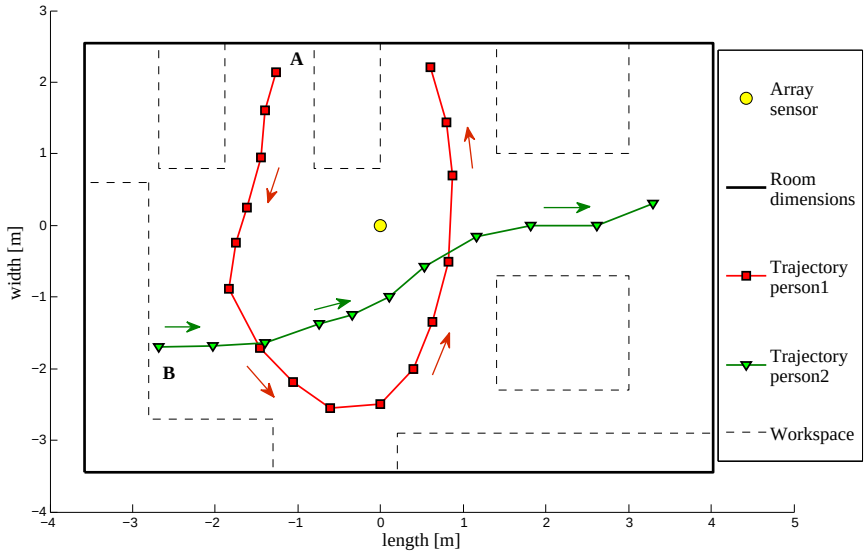

(a)

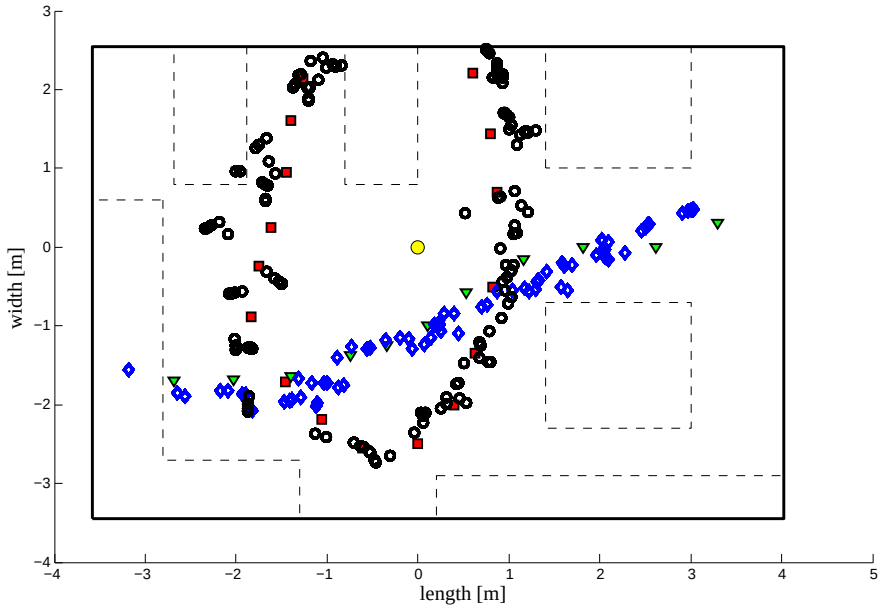

(b)

Figure 4.4: (a) Office room outline and target trajectories. ,(b) Granular detection and tracking result of the two-occupants scenario.

The movement begins by the first occupant (green triangles trajectory) starts the journey at point A; when the first occupant approaches the middle of its track, the second occupant starts from point B and walks along the red squares. The results

from the real-time location estimation and tracking are shown in Fig. 4.5(b) by red circles, blue diamonds, and black dots for the first, second and third occupant respectively.

Furthermore, the algorithm running time was measured during the experiments. It was shown that the running time per scan varies depending on the number of detected active range bins due to occupants' movement, but is shown to be less than 0.2 s based on the conducted experiments.

4.1.2.1 Discussion

It can be inferred from the the experimental results shown in Figs 2.18, 4.4(b) and 4.5(b) that the location estimates from the proposed granular presence sensing and tracking system closely matches the real occupant trajectories. Therefore, the proposed algorithm provides reliable location estimates for both single and multiple occupant scenarios in real-time.

4.2 Experimental and simulation results of the ultrasonic control messaging system

In this section, the performance of the proposed communication system is tested through experiments as well as simulations and the results are provided.

4.2.1 Experiment settings and design parameters

The experiments were performed in the same office room as explained in Section 4.1. There are 4 work-spaces in the aforementioned office room illustrated in Fig 4.6 in the x-y plane. The solid lines in this figure shows the physical room boundaries while the black dashed lines indicate the workspace regions. Furthermore, the array sensor receiver is shown with the yellow circle in approximately the middle of the room. The room is divided into 8 zones based on the azimuth angle of the received waveform by the circular array. The zones are indicated alphabetically by blue squares. The transmitter of the communication system is implemented in MATLAB and was tested on three laptop speakers with diferent maximum volume levels. The raw received signal by the circular array is first sampled and digitized and supplied to the desktop computer for further processing in MATLAB. The parameters of the transmitter are summarized in Table 4.5.

4.2.2 Experimental results

4.2.2.1 Experiments with the LOS orientation of the mobile device

In this experiment, the laptop is placed at the four different work-spaces as shown in Fig. 4.6. For the first set of tests, The orientation of the mobile device is

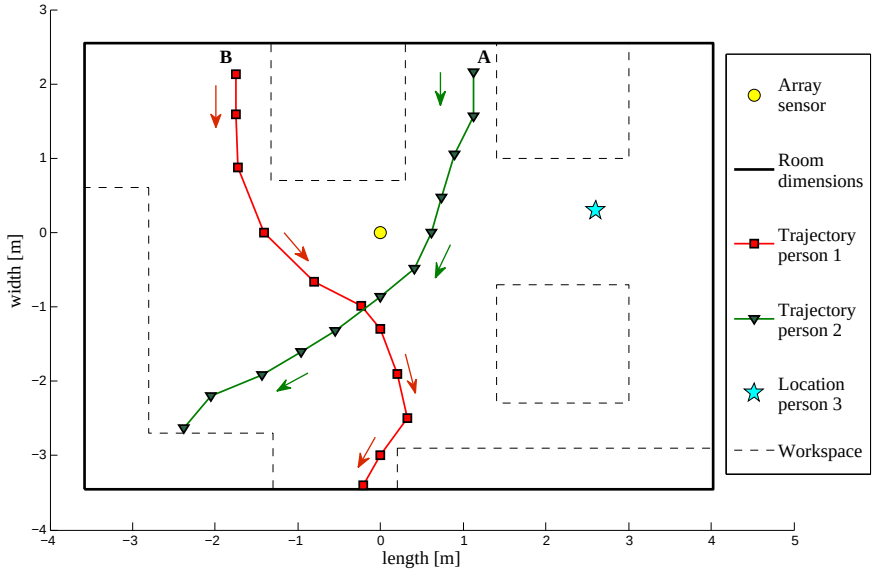

(a)

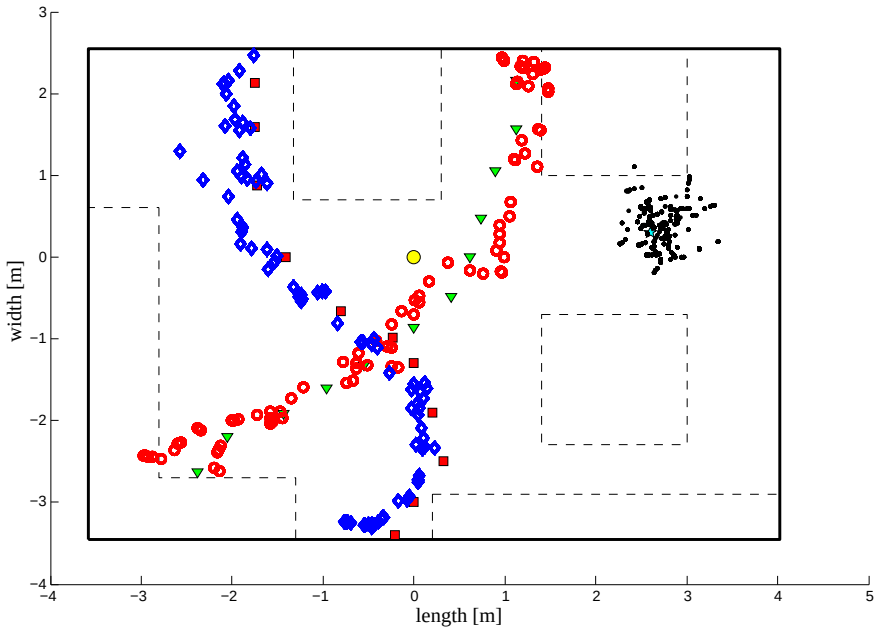

(b)

Figure 4.5: (a) Office room outline and target trajectories. ,(b) Granular detection and tracking result of three occupants scenario.

chosen such that a clear LOS path exists between the transmitter (mobile device) and the receiver array. For this scenario, the channel impulse response resembles Fig. 4.7(a). A total of 150 control commands were transmitted in all four work-

$f_{c,2}$	20 kHz
$f_{s,2}$	44.1 kHz
Modulation scheme	OOK
T_b	500 μs
L_1	5 bits
Error correcting codes	BCH(15,5,7)
B_2	1.6 kHz

Table 4.5: Communication system parameters.

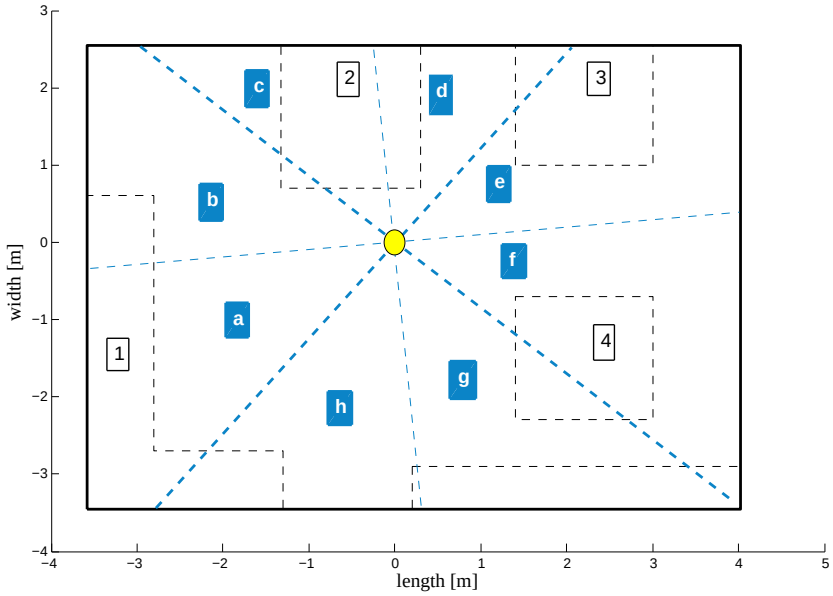

Figure 4.6: Zoning of the test office room based on azimuth angle.

space regions. The received signals are decoded and the DOA of the incoming signals were estimated in real-time. It is shown that for the first scenario, 100% of the messages are decoded correctly and the angular position of the mobile device was inferred correctly from the azimuth angle estimates.

The transmission of the data packet from the laptop speaker required approximately 1.7 s. This was due to the buffering delay of the laptop speaker. The running time of the algorithm to process a complete data packet was shown through experiments to be a maximum of 0.3 s which satisfies the real-time application requirements.

4.2.2.2 Experiments under the condition that LOS is obstructed

In the second set of tests, experiments were conducted in the same room with the same laptop as mentioned in Section 4.2.2.1. In the first set of experiments,

The mobile device was faced away from the receiver array in a position that the transmitted waveform would first hit the ceiling and after reflection, receive the circular array. The channel impulse response in this case resembles Fig 4.7(b). Furthermore, the mobile device was tested under same orientation in all four work-space regions. 150 control commands was transmitted and decoded in real-time. It was shown that about 71% of the messages were decoded correctly. Among the messages decoded with error, the zone of 96% were estimated correctly. This is due to the fact that the signal was reflected from the ceiling just above the mobile device (this can be inferred from the elevation angle estimate which was 90°in these cases). Therefore, the azimuth angle estimate was the same as the azimuth angle at the position of the mobile device.

In the second set of experiments, the orientation of the mobile device is set such that the line-of-sight is blocked. This is performed either by facing the laptop speaker on the opposite direction from the position of the array sensor and facing a near-by wall, by placing an object along the path or occupant moving along the LOS path. In this case, depending on the type of obstruction, the channel impulse response resembles Fig. 4.7(b),(c) or(d). In this figure, plot (c) shows an instance of the channel when the LOS is shadowed by the occupant inside the room, plot (d) shows the case when the laptop is set facing away from the receiver with the addition of an occupant obstructing the transmitted signal. It was shown through the experiments that in this scenario, among the 150 data packets transmitted from the four work-spaces, only 51% of the messages are received and decoded correctly. Among the erroneouss received messages, the zone of about 35% were estimated correctly. The correct zone estimates again correspond to the signals that were reflected from the ceiling directly above the laptop position.

Fig 4.8 shows the effect of blocking objects as well as deviation from LOS on the received signal. Plot (a) in this figure shows the transmitted waveform, plot (b) shows the portion of the received data that is detected by the receiver to contain information under LOS channel condition, plot (c) is the data portion when LOS is blocked by facing the laptop speaker away from the array receiver, plot (d) is the received data portion when an occupant is moving along the path, plot (e) is the channel when an obstructing object is placed along the path and plot (f) shows the case when the moving occupant is directly obscuring the transmission. As mentioned earlier in Chapter 3, ultrasound is very directional and is easily obscured by objects along the path. Therefore, the received signal possess a very poor quality under the non-LOS channel conditions.

Table 4.6 summarizes the experimental results of the communication solution

4.2.3 Simulation results

In order to simulate the effect of the indoor ultrasonic channel on the transmitted communication signal and to investigate the performance of the ultrasonic

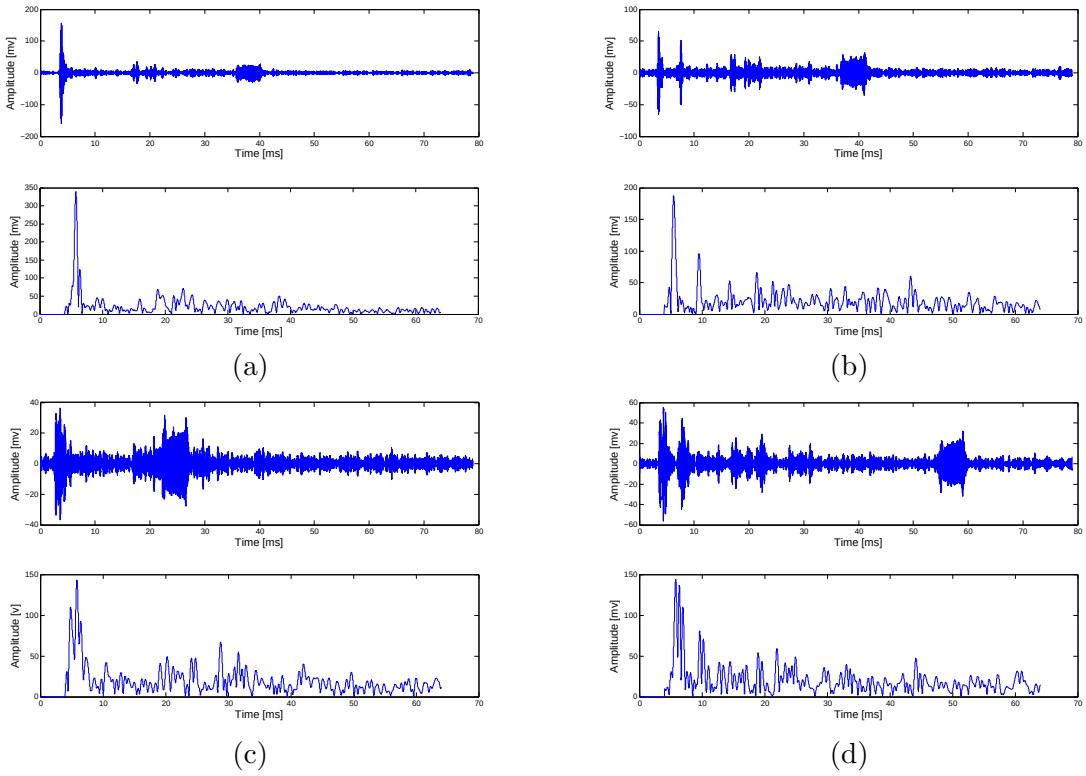

Figure 4.7: Channel impulse response. The first plot in each set represents the bandpass filtered received signal and the second plot represents the result after matched filtering (a) LOS channel, (b) LOS and shadowed channel, (c) Diffuse from the ceiling channel, (d) Diffuse and shadowed channel.

Channel condition	Transmitted	Correctly decoded	Correct zone estimate
LOS	150	150	150
Diffuse from ceiling	150	106	148
Blocked LOS	150	77	85

Table 4.6: Communication system experimental results.

communication system, we model the indoor ultrasound channel. There are three main methods to model sound propagation, namely wave-based, ray-based and statistical [85]. Ray-tracing and the image-source method, which lie in the category of ray-based models, are the most commonly used methods for the indoor airborne sound propagation. These methods are based on the geometrical room acoustics [86]. To model the impulse response of the ultrasonic channel inside the office room, using the ray-based methods, all possible sound reflection path are calculated. We use the image method of Allen and Berkley [87] to attain the room impulse response. This method models the ultrasound channel inside an empty

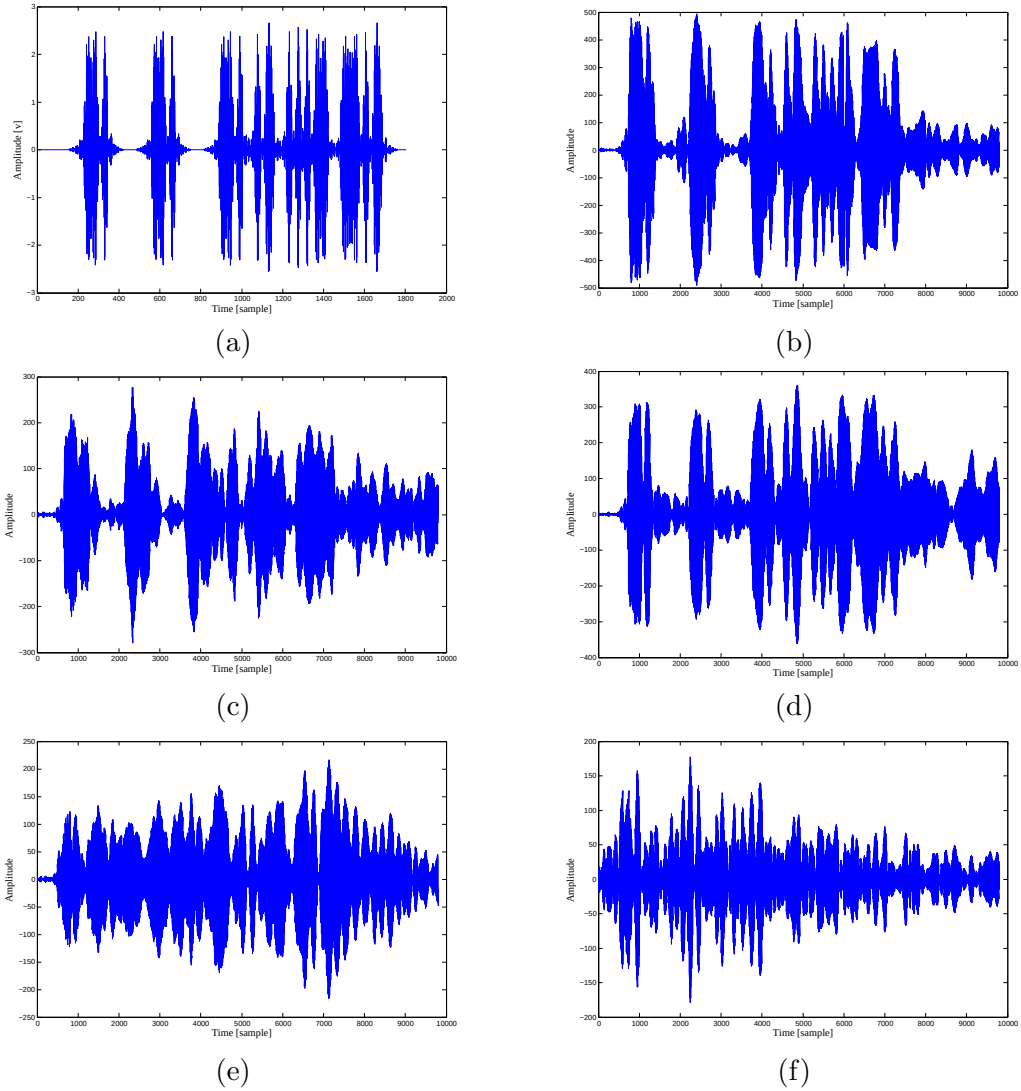

Figure 4.8: Transmitted waveform and received waveform under different channel conditions; (a) Transmitted waveform, (b) LOS channel ,(c) decodeble non-LOS channel, d) channel when there is movement in the room, (e) non-decodeable non-LOS channel, (f) channel when the moving object obscures the transmission.

room with determined dimensions. The room dimensions are chosen the same as the dimensions of the office under test as indicated in Table 4.1. The transmitter and receiver are chosen to be omnidirectional. The reverberation time (RT) of the ultrasound channel is chosen to be RT = 60 ms as is typical in building acoustics [47] and is shown to be valid in our room settings through experimental results. Image method is based on the calculation of the reflection path from planar surfaces (walls and the ceiling and the floor), to care for the furniture inside the room

we adjust the reflection order to increase the complexity of the room. We further test the system by placing the mobile transmitter at 35 different locations in the room as shown in Fig 4.9. The impulse response depends on the location of the receiver, an instance of the impulse response achieved using the simulation is shown in Fig 4.10. The performance of the communication system is tested by convolving all the 32 transmitted control commands in each location with the generated impulse response for the particular transmitter-receiver placement. Furthermore, 20 dB noise is added to the convolved result. After performing the simulations, the obtained message error rate is approximately 7 percent.

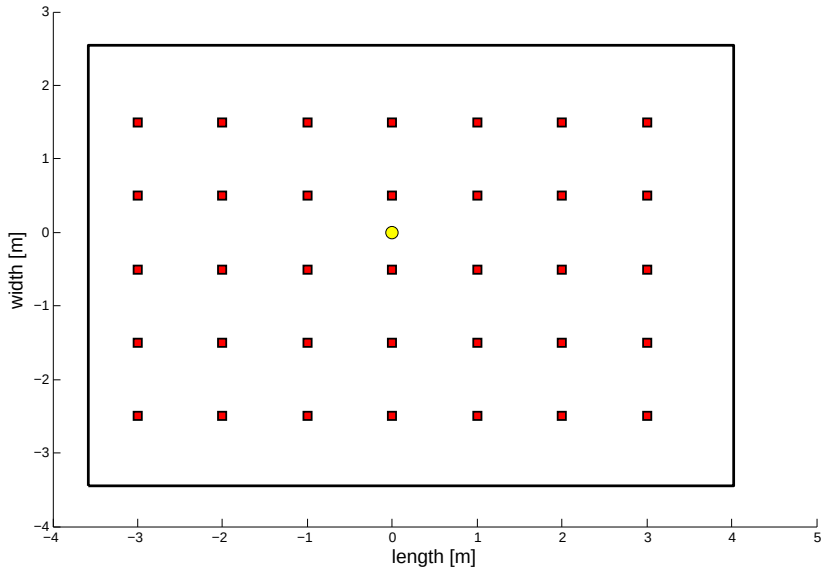

Figure 4.9: Test locations within the room.

4.2.4 Discussion

It can be deduced from the experimental and simulation results that the proposed communication system is capable of reliably decoding the received lighting control command and estimating the occupant zone under the condition that the orientation of the mobile device allows for a direct path between the transmitter and the receiver. This is due to the fact that sound in higher frequencies is very directional and easily absorbed and blocked by obstacles [52, 14]. Therefore, the quality of the received signal is highly dependant on the orientation of the speaker of the mobile device with relation to the array receiver. Furthermore, if the LOS assumption is violated, the DOA of the received signal would result in faulty arrival zone estimates due to the fact that it comes from a reflection path. Moreover, since LOS orientation is common in remote controlling applications and estimating

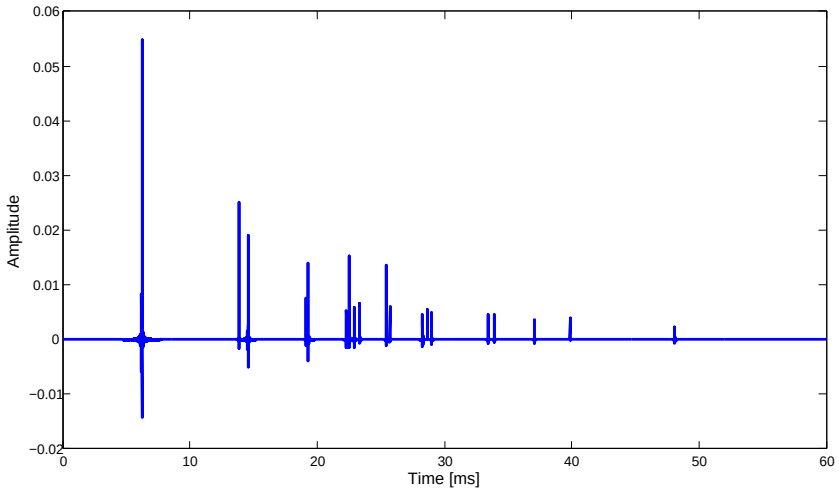

Figure 4.10: An instance of the generated room impulse response using the image method.

the occupant zone requires the existence of LOS, the design of the communication system was based on LOS assumption. Consequently, advanced receiver and encoding schemes such as interleaving and channel equalization were not considered in the design. Therefore, for the purpose of correct decoding of the lighting control command and occupant zone estimation, a direct LOS between the mobile device and the array receiver is necessary. Moreover, It was shown that by increasing the volume of the speaker, under LOS condition, the control command is correctly decoded from different distances between the mobile device and the array receiver throughout the room.

additionally, the practicality of the system is also dependant on the directionality pattern and the placement of the laptop speakers that provides the possibility of maintaining a direct path between the mobile device and the array receiver. Furthermore, on some laptops a minor audible buzzing sound is created when operating at the highest volume. This is caused due to i) the non-linearities of the laptop speakers at the maximum gain and ii) frequent transition between no sound and high frequency carrier[15]. Pulse shaping filters were applied on the transmitted pulses for amplitude tapering to reduce this buzzing sound as discussed in Chapter 3. However, the system can advantage from this buzzing sound since it provides feedback to the other occupants to avoid the simultaneous transmission from two different locations which in the latter case, would result into packet collision at the receiver.

4.3 Conclusions

In this chapter, the proposed algorithms for the granular presence sensing system as well as the ultrasonic communication system were assessed through experiments and simulation. It was shown that the presence sensing system is capable of providing accurate location estimates in real-time under single and multiple target scenarios. Furthermore, the proposed communication system for light remote controlling and occupant zone estimation was shown to achieve reliable decoding and DOA estimation performance for all distances within the room (maximum distance 6 m) under LOS orientation of the mobile device with respect to the array receiver.

5 Conclusions and Future Work

5.0.1 Conclusions

In this thesis two aspects of the smart office lighting system were considered; 1) providing coarse-grained occupancy location information, 2) a combined communication and zone estimation system for light remote controlling applications . Both systems were based on ultrasound technology and a uniform circular receiver array sensor configuration. Real-time algorithms were presented and tested in a typical office environment.

In the proposed granular occupancy localization and tracking algorithm, the range, azimuth and elevation angles corresponding to potential occupant movements were obtained after range processing and DOA estimation. The observation points were then converted to Cartesian coordinates and a 2D Kalman filter tracking based on an NCV model was applied. Furthermore, a track maintenance algorithm was employed to determine true occupant movement tracks. The algorithm was evaluated with an 8-element uniform circular receiver array prototype and a co-located single transmitter in an indoor office environment. scenarios with a single, two and three targets were tested and the results were processed in real-time. It was shown through experiments that the algorithm is caple of providing reliable location estimates with the required accuracy.

For the design of the communication solution, asynchronous communication based on OOK modulation scheme and BCH encoding for reliable communication was proposed. The operational frequency was chosen in the near-ultrasonic frequency range that can be produced by consumer laptop and smart-phones and is still inaudible to human ear. At the receiver side non-coherent detection together with DOA estimation through beam-forming was considered. The performance of the system was evaluated in real-time in an indoor office environment with an 8-element uniform circular array prototype and a laptop for signalling from the user. It was shown through experimental and simulation results that the proposed communication solution provides reliable communication and occupant zone estimation throughout the room given the line-of-sight orientation of the mobile device with regards to the receiver array is maintained.

5.0.2 Recommendations for future work

In this section some future modifications and extensions of the proposed granular presence sensing and communication solution are presented.

- Consideration for fast moving occupants

  The design of the granular presence sensing system was based on slow to moderate movement speeds of the occupants in an office environment. In practice, occupants may walk faster than 1 ms^{-1} especially in open areas like corridors. To guarantee the detection and tracking for fast moving occupants, the cut-off frequency of the low-pass filter can be adjusted accordingly.

- 3 dimensional localization and tracking

  Range and DOA estimation using a uniform circular array provides information about range, azimuth and elevation of the occupant. In this thesis, due to application, after estimating x,y and z coordinates of the target, only x and y coordinates were used and a 2D tracker was applied. However, the system is capable of 3D location estimation and tracking by applying a 3D Kalman filter-based tracker instead.

- High resolution DOA estimation techniques

  High resolution DOA estimation techniques provide DOA estimation with higher accuracy and better consistency as the number of sources increase. These techniques for circular arrays are based on phase-mode transformation of the UCA array response to a phase-mode array response with similar structure as ULA . However, the aperture size in the phase-mode space is at most half of the aperture size in element-space. Therefore, by applying the phase-mode transform, the maximum number of sources whose DOA can be unambiguously estimated reduces to half. The applicability of methods based on the sparse ruler concept [69, 88] that are primarily investigated for ULA can be considered for the beam-space array response of the UCA to restore the aperture size after beam-space transformation.

- Tracking performance improvement

  Kalman filter tracking based on NCV model and a scoring mechanism based on the received SNR and proximity of the observation point with the predicted location was proposed. However, the performance of the tracking system may be improved in a number of ways.

  First, it has been shown [63] that the linear frequency modulated (LFM) up-sweep waveform provides the best tracking performance among radar waveforms. LFM also provides better range resolution than single-frequency pulse. Therefore, by exploiting a broadband transmitter, both the range estimation and tracking performance can be increased.

  Second, a pulsed Doppler radar can provide estimate of the speed of the occupant as well as the range. The speed estimates can be used for better motion models than NCV in the tracking system.

  Third, a more advanced multiple target tracking solution may be proposed based on interacting multiple model (IMM) occupant motion model, multiple hypothesis tracking (MHT) observation-to-track allocation and a

scoring mechanism based on sequential probability ratio test (SPRT) [73] to acheive better tracking performance.

- Implementation of the communication scheme on mobile phones

  The proposed communication solution has been implemented in MATLAB and tested on laptop speakers. Prior research has shown the potentiality of ultrasonic communication on smart-phone speakers [58]. By translating the proposed communication solution into a programming language for smart-phones, the system can be tested and executed on smart-phones instead of laptops.

- Robustness against ISI and burst error

  It was shown that when the LOS orientation of the mobile device with respect to the array receiver is violated, the decoding performance degrades. In the absense of a significant LOS, multipath components cause ISI at the received signal. Moreover, due to multipath fading nature of the indoor ultrasound channel, burst errors are likely to happen. By applying channel equalization and interleaving, the resistance of the communication system against ISI and burst error may be increased.

- Messaging based on orthogonal codes

  The communication solution proposed in this thesis translates the control command into a binary sequence and en-frames the sequence for asynchronous communication. However, different commands can be translated into orthogonal bit sequences. In this case, the receiver correlates the received signal with a bank of known bit sequences to decode the message. This scheme provides a better resistance against multi-path and interference from other users and other signals present at the operating frequency. Furthermore, if two users with different requests transmit simultaneously, the command of both can be decoded.

- Improved transmitter location estimation by range information

  For the purpose of estimating the transmitter zone in the communication solution, a simple scheme based on azimuth angle was proposed. However, by estimating the range of the mobile transmitter e.g., by adding a second base station and applying trilateration, the range measurements can be combined with the estimated DOA for a more accurate location estimation.

- Combining the solutions into a smart lighting system

  In this thesis, two aspects of the indoor smart lighting system were considered, namely granular presence sensing and communication system for light remote controlling. The proposed solutions may be integrated with an illumination control scheme such as the one proposed in [4] for a complete smart indoor lighting solution.

Bibliography

[1] Prowave Electronics Corporation. Air altrasonic ceramic transducers, Online:www.prowave.com.tw/english/products/ut/ep/40ep14d.htm.

[2] Knowles Acoustics. Mini sisonic microphone specification, Online:http://www.knowles.com/search/prods_pdf/ SPM0204HD5.PDF.

[3] JF Roper. Lighting for commercial buildings. *Electronics & Power*, 12(8):297–301, 1966.

[4] David Caicedo and Ashish Pandharipande. Distributed illumination control with local sensing and actuation in networked lighting systems. *Sensors Journal, IEEE*, 13(3):1092–1104, 2013.

[5] Niels van de Meugheuvel, Ashish Pandharipande, David Caicedo, and PPJ van den Hof. Distributed lighting control with daylight and occupancy adaptation. *Energy and Buildings*, 75:321–329, 2014.

[6] Heng-Tao Wang, Qing-Shan Jia, Chen Song, Ruixi Yuan, and Xiaohong Guan. Estimation of occupancy level in indoor environment based on heterogeneous information fusion. In *Decision and Control (CDC), 2010 49th IEEE Conference on*, pages 5086–5091. IEEE, 2010.

[7] Robert Tomastik, Yiqing Lin, and Andrzej Banaszuk. Video-based estimation of building occupancy during emergency egress. In *American Control Conference, 2008*, pages 894–901. IEEE, 2008.

[8] Ashish Pandharipande and David Caicedo. Adaptive illumination rendering in led lighting systems. 2013.

[9] Meng-Shiuan Pan, Lun-Wu Yeh, Yen-Ann Chen, Yu-Hsuan Lin, and Yu-Chee Tseng. A wsn-based intelligent light control system considering user activities and profiles. *Sensors Journal, IEEE*, 8(10):1710–1721, 2008.

[10] Panayiotis Ioannides and Constantine A Balanis. Uniform circular arrays for smart antennas. *Antennas and Propagation Magazine, IEEE*, 47(4):192–206, 2005.

[11] CM Tan, P Fletcher, MA Beach, AR Nix, M Landmann, and RS Thoma. On the application of circular arrays in direction finding part i: investigation into the estimation algorithms. *1st Annual COST*, 273, 2002.

[12] Carlos Medina, José Carlos Segura, and Angel De la Torre. Ultrasound indoor positioning system based on a low-power wireless sensor network providing sub-centimeter accuracy. *Sensors*, 13(3):3501–3526, 2013.

[13] Gaetano Borriello, Alan Liu, Tony Offer, Christopher Palistrant, and Richard Sharp. Walrus: wireless acoustic location with room-level resolution using ultrasound. In *Proceedings of the 3rd international conference on Mobile systems, applications, and services*, pages 191–203. ACM, 2005.

[14] Viacheslav Filonenko, Charlie Cullen, and James D Carswell. Indoor positioning for smartphones using asynchronous ultrasound trilateration. *ISPRS International Journal of Geo-Information*, 2(3):598–620, 2013.

[15] Will Archer Arentz and Udana Bandara. Near ultrasonic directional data transfer for modern smartphones. In *Proceedings of the 13th international conference on Ubiquitous computing*, pages 481–482. ACM, 2011.

[16] Hui Liu, Houshang Darabi, Pat Banerjee, and Jing Liu. Survey of wireless indoor positioning techniques and systems. *Systems, Man, and Cybernetics, Part C: Applications and Reviews, IEEE Transactions on*, 37(6):1067–1080, 2007.

[17] Da Zhang, Feng Xia, Zhuo Yang, Lin Yao, and Wenhong Zhao. Localization technologies for indoor human tracking. In *Future Information Technology (FutureTech), 2010 5th International Conference on*, pages 1–6. IEEE, 2010.

[18] Zebra Technology Company. Wherenet technology, Online:https://www.zebra.com/us/en/solutions/technology-need/wherenet.html.

[19] Phongsak Prasithsangaree, Prashant Krishnamurthy, and PK Chrysanthis. On indoor position location with wireless lans. In *Personal, Indoor and Mobile Radio Communications, 2002. The 13th IEEE International Symposium on*, volume 2, pages 720–724. IEEE, 2002.

[20] Paramvir Bahl and Venkata N Padmanabhan. Radar: An in-building rf-based user location and tracking system. In *INFOCOM 2000. Nineteenth Annual Joint Conference of the IEEE Computer and Communications Societies. Proceedings. IEEE*, volume 2, pages 775–784. Ieee, 2000.

[21] Sudarshan S Chawathe. Low-latency indoor localization using bluetooth beacons. In *Intelligent Transportation Systems, 2009. ITSC'09. 12th International IEEE Conference on*, pages 1–7. IEEE, 2009.

[22] Carlos Medina, José Carlos Segura, and Angel De la Torre. Ultrasound indoor positioning system based on a low-power wireless sensor network providing sub-centimeter accuracy. *Sensors*, 13(3):3501–3526, 2013.

[23] Mohamed R Mahfouz, Cemin Zhang, Brandon C Merkl, Michael J Kuhn, and Aly E Fathy. Investigation of high-accuracy indoor 3-d positioning using

uwb technology. *Microwave Theory and Techniques, IEEE Transactions on*, 56(6):1316–1330, 2008.

[24] Sverre Holm. Hybrid ultrasound-rfid indoor positioning: Combining the best of both worlds. In *RFID, 2009 IEEE International Conference on*, pages 155–162. IEEE, 2009.

[25] Valtteri Takala and Matti Pietikainen. Multi-object tracking using color, texture and motion. In *Computer Vision and Pattern Recognition, 2007. CVPR'07. IEEE Conference on*, pages 1–7. IEEE, 2007.

[26] Roy Want, Andy Hopper, Veronica Falcao, and Jonathan Gibbons. The active badge location system. *ACM Transactions on Information Systems (TOIS)*, 10(1):91–102, 1992.

[27] Nissanka B Priyantha, Anit Chakraborty, and Hari Balakrishnan. The cricket location-support system. In *Proceedings of the 6th annual international conference on Mobile computing and networking*, pages 32–43. ACM, 2000.

[28] Cambridge University Computer Laboratory. The bat ultrasonic location system, Online:http://www.cl.cam.ac.uk/research/dtg/attarchive/bat/.

[29] Sverre Holm. Robust ultrasonic indoor positioning system with high accuracy, March 23 2011. US Patent App. 13/636,522.

[30] Hans J Keller. Advanced passive infrared presence detectors as key elements in integrated security and building automation systems. In *Security Technology, 1993. Security Technology, Proceedings. Institute of Electrical and Electronics Engineers 1993 International Carnahan Conference on*, pages 75–77. IEEE, 1993.

[31] Sverre Holm. Airborne ultrasound data communications: The core of an indoor positioning system. In *Proc IEEE Ultrasonics Symposium, Rotterdam, Netherlands*, 2005.

[32] Yasuhiro Fukuju, Masateru Minami, Hiroyuki Morikawa, and Tomonori Aoyama. Dolphin: An autonomous indoor positioning system in ubiquitous computing environment. In *WSTFEUS*, pages 53–56, 2003.

[33] Greg Welch and Eric Foxlin. Motion tracking survey. *IEEE Computer graphics and Applications*, pages 24–38, 2002.

[34] Sebastian Thrun, Dieter Fox, Wolfram Burgard, and Frank Dellaert. Robust monte carlo localization for mobile robots. *Artificial intelligence*, 128(1):99–141, 2001.

[35] Chris Hand. A survey of 3d interaction techniques. In *Computer graphics forum*, volume 16, pages 269–281. Wiley Online Library, 1997.

[36] Cristina Videira Lopes and Pedro MQ Aguiar. Acoustic modems for ubiquitous computing. *IEEE pervasive computing*, 2(3):62–71, 2003.

[37] John D Stolshek and Philip A Koehring. Ultrasonic technology provides for control of lighting. *Industry Applications, IEEE Transactions on*, (6):1564–1572, 1984.

[38] Adrian Lin and Hao Ling. Doppler and direction-of-arrival (ddoa) radar for multiple-mover sensing. *IEEE transactions on aerospace and electronic systems*, 43(4):1496–1509, 2007.

[39] David Caicedo and Ashish Pandharipande. Ultrasonic array sensor for indoor presence detection. In *Signal Processing Conference (EUSIPCO), 2012 Proceedings of the 20th European*, pages 175–179. IEEE, 2012.

[40] Ryan Melfi, Ben Rosenblum, Bruce Nordman, and Ken Christensen. Measuring building occupancy using existing network infrastructure. In *Green Computing Conference and Workshops (IGCC), 2011 International*, pages 1–8. IEEE, 2011.

[41] David Caicedo and Ashish Pandharipande. Ultrasonic arrays for localized presence sensing. *Sensors Journal, IEEE*, 12(5):849–858, 2012.

[42] David Caicedo and Ashish Pandharipande. Distributed ultrasonic zoned presence sensing system. 2014.

[43] DEN Davies. Circular arrays. *The handbook of antenna design*, 2:299–329, 1983.

[44] Chuan Li, David A Hutchins, and Roger J Green. Short-range ultrasonic digital communications in air. *Ultrasonics, Ferroelectrics and Frequency Control, IEEE Transactions on*, 55(4):908–918, 2008.

[45] Chuan Li, David A Hutchins, and Roger J Green. Short-range ultrasonic communications in air using quadrature modulation. *Ultrasonics, Ferroelectrics and Frequency Control, IEEE Transactions on*, 56(10):2060–2072, 2009.

[46] Chuan Li, David A Hutchins, and Roger J Green. Response of an ultrasonic communication channel in air. *IET communications*, 6(3):335–343, 2012.

[47] Sverre Holm, Ole B Hovind, Svein Rostad, and Rune Holm. Indoor data communications using airborne ultrasound. In *Acoustics, Speech, and Signal Processing, 2005. Proceedings.(ICASSP'05). IEEE International Conference on*, volume 3, pages iii–957. IEEE, 2005.

[48] Wentao Jiang and William MD Wright. Wireless communication using ultrasound in air with parallel ook channels. 2013.

[49] Tarig Ballal, Mohamed M Saad, and Chris Bleakley. Design and implementation of an indoor ultrasonic communication system. 2011.

[50] H Haynes and M Akeman. Final report, ultrasonic communication project, phase 1, fy 1999. *Engineering Technology Division, Oak Ridge National Laboratory, Tech. Rep*, 2000.

[51] Robert A Zurek, Aaron Dietrich, and Michael L Charlier. Omnidirectional ultrasonic communication system, March 26 2002. US Patent 6,363,139.

[52] Viacheslav Filonenko, Charlie Cullen, and James Carswell. Investigating ultrasonic positioning on mobile phones. In *Indoor Positioning and Indoor Navigation (IPIN), 2010 International Conference on*, pages 1–8. IEEE, 2010.

[53] Chunyi Peng, Guobin Shen, Yongguang Zhang, Yanlin Li, and Kun Tan. Beepbeep: a high accuracy acoustic ranging system using cots mobile devices. In *Proceedings of the 5th international conference on Embedded networked sensor systems*, pages 1–14. ACM, 2007.

[54] Marius H Hennecke and Gernot A Fink. Towards acoustic self-localization of ad hoc smartphone arrays. In *Hands-free Speech Communication and Microphone Arrays (HSCMA), 2011 Joint Workshop on*, pages 127–132. IEEE, 2011.

[55] Bingsheng Zhang, Qin Zhan, Junfei Wang, Kui Ren, Cong Wang, and Di Ma. Priwhisper: Enabling keyless secure acoustic communication for smartphones.

[56] Electronics Bus. Ultrasonic communication system of mobile data transfer using zoosh, Online:http://electronicsbus.com/ultrasonic-communication-system-mobile-data-transfer-zoosh/.

[57] Harvest Zhang and Bonnie Eisenman. Squeakychat: Ultrasonic communication using commercial notebook computers.

[58] Quitenet, Online:https://github.com/Katee/quietnet.

[59] Boris Smus. Sonicnet, Online:http://smus.com/ultrasonic-networking/.

[60] Hamid Krim and Mats Viberg. Two decades of array signal processing research: the parametric approach. *Signal Processing Magazine, IEEE*, 13(4):67–94, 1996.

[61] Mark A Richards, Jim Scheer, and William A Holm. *Principles of modern radar: basic principles*. SciTech Pub., 2010.

[62] Samuel Blackrnan and Artech House. Design and analysis of modern tracking systems. *Boston, MA: Artech House*, 1999.

[63] Ruixin Niu, Peter Willett, and Yaakov Bar-Shalom. Tracking considerations in selection of radar waveform for range and range-rate measurements. *Aerospace and Electronic Systems, IEEE Transactions on*, 38(2):467–487, 2002.

[64] Constantine A Balanis. *Antenna theory: analysis and design*. John Wiley & Sons, 2012.

[65] Tie-Jun Shan, Mati Wax, and Thomas Kailath. On spatial smoothing for direction-of-arrival estimation of coherent signals. *IEEE Transactions on Acoustics, Speech, and Signal Processing*, 33(4):806–811, 1985.

[66] Monson H Hayes. *Statistical digital signal processing and modeling*. John Wiley & Sons, 2009.

[67] Cherian P Mathews and Michael D Zoltowski. Eigenstructure techniques for 2-d angle estimation with uniform circular arrays. *Signal Processing, IEEE Transactions on*, 42(9):2395–2407, 1994.

[68] Reiner S Thoma, Dirk Hampicke, Andreas Richter, Gerd Sommerkorn, Axel Schneider, Uwe Trautwein, and Walter Wirnitzer. Identification of time-variant directional mobile radio channels. *Instrumentation and Measurement, IEEE Transactions on*, 49(2):357–364, 2000.

[69] Siavash Shakeri, Dyonisius Dony Arianandа, and Geert Leus. Direction of arrival estimation using sparse ruler array design. In *Signal Processing Advances in Wireless Communications (SPAWC), 2012 IEEE 13th International Workshop on*, pages 525–529. IEEE, 2012.

[70] Hervé Sizun and Pierre de Fornel. *Radio wave propagation for telecommunication applications*. Springer, 2005.

[71] Henry E Bass and Lee N Bolen. Ultrasonic background noise in industrial environment. *The Journal of the Acoustical Society of America*, 79(S1):S59–S59, 1986.

[72] Mark A Richards. *Fundamentals of radar signal processing*. Tata McGraw-Hill Education, 2005.

[73] Samuel S Blackman. Multiple hypothesis tracking for multiple target tracking. *Aerospace and Electronic Systems Magazine, IEEE*, 19(1):5–18, 2004.

[74] X Rong Li and Vesselin P Jilkov. Survey of maneuvering target tracking. part i. dynamic models. *Aerospace and Electronic Systems, IEEE Transactions on*, 39(4):1333–1364, 2003.

[75] Yaakov Bar-Shalom and Xiao-Rong Li. *Estimation and tracking: principles, techniques, and software*, volume 393. Artech House Boston, 1993.

[76] Robert Resnick, David Halliday, and J Walker. *Fundamentals of physics*. John Wiley, 1988.

[77] Edward A Lee and David G Messerschmitt. *Digital communication*. Kluwer, 1994.

[78] K Sam Shanmugam. Digital and analog communication systems. *NASA STI/Recon Technical Report A*, 80:23225, 1979.

[79] John G Proakis. Digital communications, 1995.

[80] Marvin K Simon and Mohamed-Slim Alouini. *Digital communication over fading channels*, volume 95. John Wiley & Sons, 2005.

[81] I Greenberg. Retraining wlan receivers for ofdm operation. *Communication Systems Design*, 8, 2002.

[82] K Wang, M Faulkner, J Singh, and I Tolochko. Timing synchronization for 802.11 a wlans under multipath channels. In *Proc. ATNAC*, volume 2004, 2003.

[83] Fernando Seco Granja and Antonio Ramón Jiménez. Ultrasound modulation and codification for localization systems. *Biblioteca de Ciencias: New Acoustics: selected topics II*, pages 167–186, 2006.

[84] Klaus Witrisal, Geert Leus, Gerard JM Janssen, Marco Pausini, Florian Trösch, Thomas Zasowski, and Jac Romme. Noncoherent ultra-wideband systems. *Signal Processing Magazine, IEEE*, 26(4):48–66, 2009.

[85] Lauri Savioja, Jyri Huopaniemi, Tapio Lokki, and Ritta Väänänen. Creating interactive virtual acoustic environments. *Journal of the Audio Engineering Society*, 47(9):675–705, 1999.

[86] Heinrich Kuttruff. *Room acoustics*. CRC Press, 2009.

[87] Jont B Allen and David A Berkley. Image method for efficiently simulating small-room acoustics. *The Journal of the Acoustical Society of America*, 65(4):943–950, 1979.

[88] Dyonisius Dony Ariananda and Geert Leus. Direction of arrival estimation for more correlated sources than active sensors. *Signal Processing*, 93(12):3435–3448, 2013.

System Specifications

A

In this appendix, some of the features of the ultrasonic transmitter and receiver which are relevant to the design of our systems are presented. Most of the information is extracted from the components datasheet [2, 1].

A.1 Transmitter model

The transmitter used in the indoor granular presence sensing system is of model 400EP14D, depicted in Fig A.1.The specifications of the transmitter are summarized in Table A.1. The azimuth (wide) angle and the elevation (narrow) angle beam-pattern of the transmitter are depicted in Fig A.2

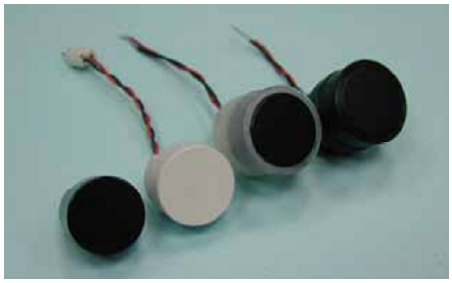

Figure A.1: Air ultrasonic ceramic transducer[1].

Name	Air ultrasonic ceramic transducer
Model	400EP14D
Center frequency	40.0 $\pm$ 1 kHz
Bandwidth	2 kHz
Azimuth beam angle	125°
Elevation beam angle	65°
Maximum driving voltage	100 Vpp

Table A.1: Specifications of the transmitter [1].

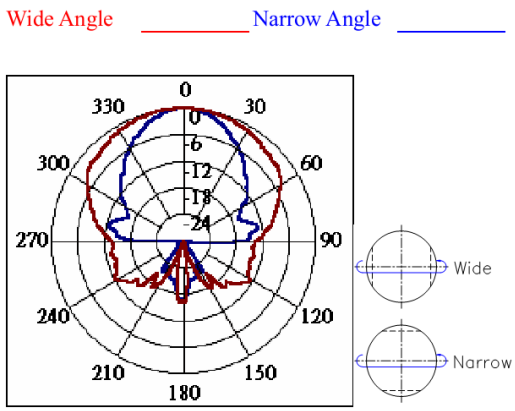

Figure A.2: Beam pattern of the transmitter (tested at 40 KHz)[1]..

A.2 Receiver model

The ultrasonic receiver used in the indoor granular presence sensing system as well as the communication system is composed of 8 elements of model SPM0204HD5 as discussed in the following sections.

A.2.1 Receiver element specifications

Each receiver element in the circular array receiver has a recyangular shape as depicted in Fig A.3. The parameters of each element is summerized in Table A.2. The frequency response of the receiver element is shown in Fig A.4. As can be inferred from the figure, the receiver has a wide operational frequency range.

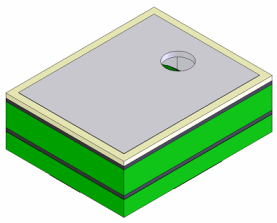

Figure A.3: One receiver element [2].

Name	Mini SiSonic Microphone
Model	SPM0204HD5
Frequency range	100 Hz-80 kHz
Directionality	Omnidirectional

Table A.2: Specifications of one element of the receiver [2].

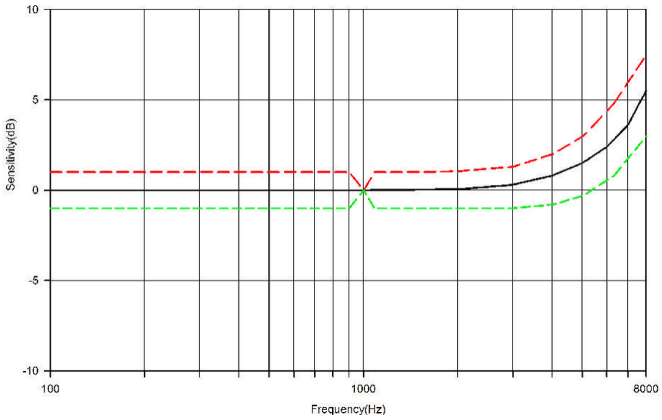

Figure A.4: Frequency response curve of one receiver element [2].

A.2.2 Array receiver design constraints

The dimensions of each receiver element is shown in Fig A.5. The width of each receiver element is about 3.76 mm. Therefore, positioning the elements in an octagonal geometry poses a constraint on the minimum possible distance between the center of the elements to be 4.614 mm.

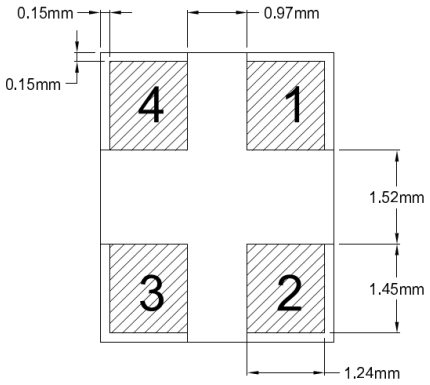

Figure A.5: Mechanical schematic of a receiver element.

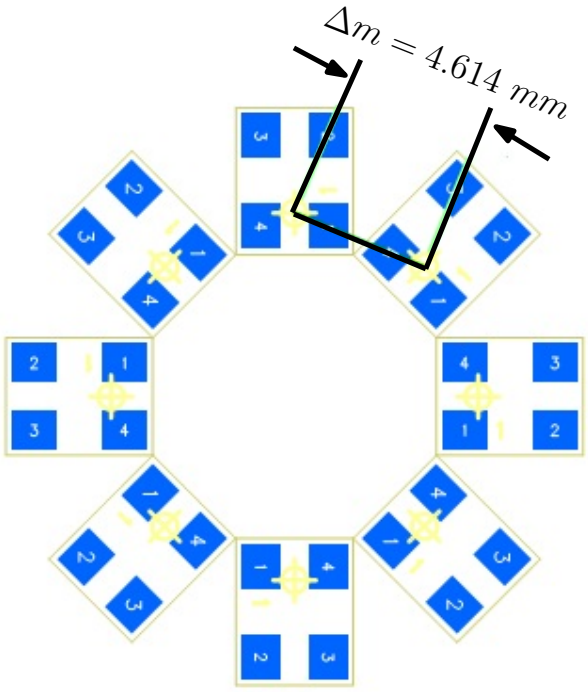

Figure A.6: Array receiver design schematic.